
The redshifted selected sample of long gamma-ray burst host galaxies: the complete metallicity measurements at $z \leq 0.41^{*\dagger}$

Yuu NIINO¹, Kentaro AOKI², Tetsuya HASHIMOTO¹, Takashi HATTORI², Shogo ISHIKAWA³, Nobunari KASHIKAWA¹, George KOSUGI¹, Masafusa ONOUE³, Jun TOSHIKAWA¹, and Kiyoto YABE⁴

¹National Astronomical Observatory of Japan, 2-21-1 Osawa, Mitaka, Tokyo 181-8588, Japan

²Subaru Telescope, National Astronomical Observatory of Japan, 650 North Aohoku Place, Hilo, HI 96720, USA

³Department of Astronomy, School of Science, SOKENDAI (The Graduate University for Advanced Studies), 2-21-1 Osawa, Mitaka, Tokyo 181-8588, Japan

⁴Kavli Institute for the Physics and Mathematics of the Universe, The University of Tokyo, Kashiwanoha, Kashiwa 277-8583, Japan

*E-mail: yuu.niino@nao.ac.jp

Received (reception date); Accepted (acceptation date)

Abstract

We present the complete list of host galaxy metallicities for all long GRBs whose redshifts were determined to be ≤ 0.41 before the end of March 2014, including newly obtained spectroscopic datasets of the host galaxies of GRB 060614, 090417B, and 130427A. We compare the metallicity distribution of the redshift selected complete sample to the model predictions, and constrain the relation between metallicity and GRB occurrence. We take account of spatial variation of metallicities among star forming regions within a galaxy. We found that the models, in which only low-metallicity stars produce GRBs with a sharp cutoff of GRB production efficiency around $12+\log(\text{O}/\text{H}) \sim 8.2$, can well reproduce the observed distribution, while the models with moderate (or no) metallicity dependence are not consistent with the observations. This is the first fair estimate of the metallicity distribution of GRB host galaxies based on the redshift selected complete sample in the *Swift* era. We also discuss possible sampling biases we may suffer by collecting long GRBs whose redshifts are known, presenting the photometric observations of the host galaxy of GRB 111225A at $z = 0.297$ whose redshift has been undetermined until ~ 2.3 years after the burst.

Key words: gamma-ray burst: individual — gamma-ray burst: general — galaxies: abundances — galaxies: star formation

* Based on observations obtained at the Gemini Observatory via the time exchange program between Gemini and the Subaru Telescope (processed using the Gemini IRAF package), which is operated by the Association of Universities for Research in Astronomy, Inc., under a cooperative agreement with the NSF on behalf of the Gemini partnership: the National Science Foundation (United States), the National Research Council (Canada), CONICYT (Chile), Ministerio de Ciencia, Tecnología e

Innovación Productiva (Argentina), and Ministério da Ciência, Tecnologia e Inovação (Brazil).

† Based in part on data collected at Subaru Telescope, which is operated by the National Astronomical Observatory of Japan.

1 Introduction

A long gamma-ray burst (GRB) is one of the most energetic explosions in the universe, which is observed via soft gamma-ray emission followed by afterglow in lower energy range. It is now broadly agreed that at least some of long GRBs originate in core-collapse of massive stars together with core-collapse supernovae (CC SNe). However, CC SNe do not always accompany long GRBs, and the criteria discriminating between long GRBs and general CC SNe is one of the most important questions regarding long GRBs.

Some theoretical studies on the origin of long GRBs using stellar evolution models suggest that low-metallicity may be a necessary condition for a long GRB to occur ($Z < \text{a few} \times 0.1Z_{\odot}$, e.g. Yoon & Langer 2005; Hirschi et al. 2005; Woosley & Heger 2006). Metallicity distribution of long GRB host galaxies provides us with an important clue to study the relation between metallicity and a long GRB occurrence. Although metallicity of a long GRB host galaxy is not necessarily identical to that of the progenitor (e.g., Niino et al. 2011; Niino 2011; Levesque et al. 2011; Niino et al. 2015), galaxies with low-metallicity would have higher GRB production efficiency [i.e., long GRB rate to star formation rate (SFR) ratio] than high-metal galaxies if low-metallicity is a necessary condition for a long GRB to occur.

With a sample of 5 host galaxies (3 long GRBs and 2 X-ray flashes, XRFs), Stanek et al. (2006, hereafter S06) showed that the metallicity distribution of the host galaxies at redshifts ≤ 0.25 is significantly biased towards low-metallicities compared with star forming galaxies at similar redshifts, suggesting long GRBs really occur in low-metallicity environment. However their sample is too small to determine the relation between metallicity and long GRB occurrence rate. The sample number of spectroscopically studied long GRB host galaxy has been dramatically increased during the 10 years after S06 (e.g., Savaglio et al. 2009; Levesque et al. 2010b; Graham & Fruchter 2013). However, the relation between metallicity and long GRB occurrence rate is not understood quantitatively. One difficulty is that we can determine redshifts and/or identify host galaxies of only a small fraction of long GRBs ($\sim 30\%$ in recent observations), which is likely biased with respect to the distributions of redshifts and host galaxy properties (the z -determination/host-identification bias). Furthermore, even when the redshift and the host galaxy of a long GRB are known, the host galaxy is not always studied in detail. The targets of the spectroscopic studies have been selected non-uniformly by numerous independent researchers making the effect of the sampling bias unevaluable (the reporting bias, e.g., Graham & Fruchter 2013).

There have been some previous long GRB host observation campaigns invented to overcome the sampling biases (so called unbiased surveys, Hjorth et al. 2012; Salvaterra et al. 2012; Perley et al. 2016a). However, the samples are selected

without using informations about redshifts and host galaxies in the unbiased surveys to avoid the z -determination/host-identification bias. As a result, the samples of these surveys span a very wide range of redshifts ($z \sim 0-6$), and the properties of the host galaxies in the unbiased sample is largely affected by the redshift evolution of galaxy properties in addition to the environmental requirements for a long GRB occurrence which we try to investigate.

Some recent studies pick out GRB host galaxies in specific ranges of redshifts from the unbiased surveys and compared their properties to those of general galaxies at similar redshifts (Schulze et al. 2015; Vergani et al. 2015; Perley et al. 2016b; Japelj et al. 2016). However, because the unbiased surveys span a wide range of redshifts, the sample number becomes small when the discussion is focused on a narrow range of redshifts. The sample number is especially small at low-redshifts (< 5 GRBs at $z < 0.5$) because the cosmic long GRB rate density is low and the comoving volume element is small, although long GRB host galaxies at low-redshifts are of special importance to understand the relation between metallicity and long GRB occurrence rate as we describe below.

On the other hand, the properties of general galaxies, to which we compare long GRB host galaxies to investigate the environmental requirements for a long GRB occurrence, are still not well understood at high-redshifts. Metallicity measurement of high-redshift galaxies is an especially challenging issue (at $z \gtrsim 1$, e.g., Kewley et al. 2013; Maier et al. 2015). Hence, although the unbiased surveys are important to understand what bias we would suffer by selecting long GRBs whose redshifts and host galaxies are known, it is difficult to unveil the environmental requirements for a long GRB occurrence only with the unbiased surveys.

The complete metallicity measurements of the host galaxies of all long GRBs known at low-redshifts ($z \lesssim 0.5$) can dramatically improve our understanding of the relation between metallicity and long GRB occurrence rate. There are advantages of studying GRB host galaxies at low-redshift in some aspects.

1. The success rate of GRB redshift-determinations/host-identifications would be higher at lower redshifts (i.e., the z -determination/host-identification bias is weaker), because faint galaxies can be detected without very deep observations and spectroscopies of host galaxies can provide redshift informations even when GRB afterglows are not bright enough for spectroscopies.
2. The reporting bias can be eliminated by finding host galaxies of all GRBs known in the redshift range and completing the metallicity measurements of the host galaxies, which is difficult to do at higher redshifts ($z \gtrsim 0.5$).
3. A wealth of spectroscopic studies of general galaxies at low-redshifts, such as the Sloan Digital Sky Survey (SDSS), provides us with control sample of galaxy properties, to which

Table 1. Strategies of current long GRB host studies

sampling	bias	sample number at $z < 0.5$
incomplete	z -determination/host-identification reporting	~ 10
unbiased	none	< 5
redshift selected [†]	z -determination/host-identification (weaker at lower-redshifts)	$\gtrsim 10$

[†] This work.

we can compare long GRB host properties to investigate the relation between long GRB rate and metallicity.

The advantages and the disadvantages of the redshift selected complete study of GRB host galaxies can be summarized as in table 1, in comparison with the other strategies of GRB host studies.

Here, we present spectroscopic metallicity measurements of the host galaxies of three low-redshift GRBs, 060614, 090417B, and 130427A. Together with the spectroscopic data collected from the literature, our data provides the complete list of host metallicities for all long GRBs whose redshifts are spectroscopically determined to be ≤ 0.41 before the end of March 2014. We compare the metallicity distribution of the complete sample to the predictions of empirical models of galaxies, and constrain the relation between metallicity and GRB occurrence rate.

This paper is organized as follows. We describe our sample selection, observations, and analysis of the obtained spectra in section 2, 3, and 4, respectively. In section 5, we discuss the properties of the low-redshift long GRB host galaxies including the complete list metallicities. In section 6, we describe models of galaxy metallicity distributions, to which we compare the low-redshift sample of host galaxies to constrain the relation between metallicity and GRB occurrence rate. The results of the comparison are presented in section 7. In section 8, we discuss uncertainties of our galaxy model, possible subpopulations in the low-redshift GRBs, and sampling biases we may suffer by collecting long GRBs with known redshifts. We summarize our conclusions in section 9.

Throughout this paper, we assume the fiducial cosmology with $\Omega_\Lambda = 0.7$, $\Omega_m = 0.3$, and $H_0 = 70 \text{ km s}^{-1} \text{ Mpc}^{-1}$. The magnitudes are given in the AB system.

2 Sample selection

We collect low-redshift GRBs from online databases: Swift Gamma-Ray Burst Table¹, Gamma-Ray Burst Online Index (GRBOX)², ‘‘GRBs localized’’ with³, and GRB Host Studies

(GHOSTS)⁴. Although there are various classes of gamma-ray burst like events: e.g., long GRBs, short GRBs, ultra-long GRBs, and XRFs, we focus on host galaxies of long GRBs in this study. The classification of burst events are still controversial (e.g., Zhang et al. 2007; Bromberg et al. 2013; Levan et al. 2014a), and important burst properties for the classification such as burst duration T_{90} , and spectral peak energy E_{peak} are uncertain in some cases. However, for simplicity, we select long GRBs simply by reported T_{90} and E_{peak} as follows. The prompt emission properties are taken from Butler et al. (2007)⁵, Troja et al. (2006), Zhang et al. (2009), and Zhang et al. (2012), in addition to the online databases mentioned above.

First, we collect bursts with $2 \leq T_{90} \leq 10^4$ sec as long GRBs, considering those with $T_{90} < 2$ sec as short GRBs and $T_{90} > 10^4$ sec as ultra-long GRBs. We also exclude short GRBs with extended emissions, GRB 050709, 050724, 061210, and 071227 from our sample. From the bursts which meet the duration criteria, we remove bursts with very soft spectra (XRFs) which may be a different population from long GRBs. XRFs are often defined according to their hardness ratio which depends on energy bands of X-ray detectors. To discuss burst events discovered by various instruments, we define bursts with $E_{\text{peak}} < 40$ keV as XRFs in this study. For some *Swift* detected bursts, E_{peak} estimation is not available. In that case, we distinguish GRBs and XRFs using photon spectral index in the energy range of *Swift*-BAT (Γ_{ph}). We consider bursts with $\Gamma_{\text{ph}} \leq 1.8$ which is typical of long GRBs with $E_{\text{peak}} \geq 40$ keV (Zhang et al. 2007; Sakamoto et al. 2009) as long GRBs, and those with $\Gamma_{\text{ph}} > 1.8$ as XRFs.

Within the criteria described above, there are 13 long GRBs (hereafter, GRB means long GRB unless otherwise stated) whose redshifts are determined to be $z \leq 0.41$ before the end of March 2014 (Table 2), and 3 of them (GRB 060614, 090417B, and 130427A) are without sufficient spectroscopic observations to significantly constrain their host metallicity.

3 Observations

To measure metallicity of the host galaxies of GRB 060614, 090417B, and 130427A, we perform optical spectroscopy of the host galaxies with the Gemini Multi-Object Spectrographs (GMOS, Hook et al. 2004), and use flux ratios of the emission lines: [O II] λ 3727, H β , [O III] λ 4959, [O III] λ 5007, H α , and [N II] λ 6584, as metallicity indicators (hereafter, [O II], [O III], and [N II] mean [O II] λ 3727, [O III] λ 5007, and [N II] λ 6584, respectively, unless otherwise stated). Emission line fluxes of the GRB 130427A host galaxy obtained during a target-of-opportunity program (TOO, PI: N. Kawai) using Subaru/FOCAS (Kashikawa et al. 2002) are presented together.

¹ http://swift.gsfc.nasa.gov/archive/grb_table/

² <http://www.astro.caltech.edu/grbox/grbox.php>

³ <http://www.mpe.mpg.de/jcg/grbgen.html>

⁴ <http://www.grbhosts.org/>

⁵ <http://butler.lab.asu.edu/Swift/>

Table 2. Long GRBs at $z \leq 0.41$

GRB	redshift	source of redshift [†]
980425	0.0085	host galaxy [1]
060505	0.089	host galaxy [2]
031203	0.105	host galaxy [3]
060614	0.125	host galaxy [4, 5]
030329	0.169	afterglow, host galaxy [6]
120422A	0.283	afterglow [7], host galaxy [8]
050826	0.296	host galaxy [9]
130427A	0.340	afterglow [10], host galaxy [11]
090417B	0.345	host galaxy [12]
061021	0.346	afterglow [13], host galaxy [14]
011121	0.362	host galaxy [15, 16]
120714B	0.398	afterglow, host galaxy [17]
020819B	0.410	host galaxy [18]

Long GRBs whose redshifts are spectroscopically determined to be $z \leq 0.41$ before the end of Mar. 2014. Short GRBs, XRFs, and ultra-long GRBs are not included.

[†] If ‘host galaxy’, the redshift is determined by emission lines of the host galaxy. If ‘afterglow’, the redshift is determined by absorption lines in the afterglow. The numbers in the square brackets are the references as listed below.

References: 1. Tinney et al. (1998), 2. Ofek et al. (2006), 3. Prochaska et al. (2003), 4. Price et al. (2006), 5. Fugazza et al. (2006), 6. Greiner et al. (2003), 7. Schulze et al. (2012), 8. Tanvir et al. (2012), 9. Halpern & Mirabal (2006), 10. Levan et al. (2013), 11. Xu et al. (2013a), 12. Berger & Fox (2009), 13. Fynbo et al. (2009), 14. Hjorth et al. (2012), 15. Infante et al. (2001), 16. Garnavich et al. (2003), 17. Fynbo et al. (2012), 18. Jakobsson et al. (2005)

We also performed imaging observations of the host galaxy of GRB 111225A which we discuss in section 8.3. We describe the observations of each target in the following subsections. See table 3 for the summary of our observations.

The data were reduced in a standard manner using PyRAF⁶/IRAF⁷, together with the Gemini IRAF package and the FOCASRED package. The spectra obtained with GMOS were calibrated using spectroscopic standard stars observed on different nights, and hence the absolute flux scale is not accurate.

3.1 Spectroscopy of the GRB 060614 host galaxy

GRB 060614 is known as a GRB unassociated with a bright SN at $z = 0.125$ (Gehrels et al. 2006; Fynbo et al. 2006; Della Valle et al. 2006; Gal-Yam et al. 2006). Although some spectroscopic observations of the GRB 060614 host galaxy were performed previously (Fynbo et al. 2006; Della Valle et al. 2006; Gal-Yam et al. 2006), the metallicity measurements were uncertain because the fluxes of [N II] and [O II] lines were not well constrained.

⁶ PyRAF is a product of the Space Telescope Science Institute, which is operated by AURA for NASA

⁷ IRAF is distributed by the National Optical Astronomy Observatories, which are operated by the Association of Universities for Research in Astronomy, Inc., under cooperative agreement with the National Science Foundation.

We performed spectroscopy of the GRB 060614 host galaxy with GMOS-South using the 1.''0 slit and two different settings of grisms and order-cut filters. One is the B600 grating (no-filter) which covers 3500–6000 Å, and the other is the R400 grating + the OG515 order-cut filter covering 5300–9000 Å. The signals were 2×2 pixels binned. The B600 spectroscopy was performed on 2015 April 25 (UT). The integration time was 1000 sec \times 6, and the slit position angle was set to the parallactic angle to minimize the effect of differential atmospheric refraction. The R400 spectroscopy was performed on 2015 April 28, and May 14 with the integration time of 1200 sec \times 8 and the position angle set to the parallactic angle.

3.2 Spectroscopy of the GRB 090417B host galaxy

GRB 090417B is an optically dark GRB at $z = 0.345$ with a very long duration of > 2130 sec (Holland et al. 2010). The spectroscopy was performed with GMOS-North on 2015 March 25. We use the 1.''0 slit, the R831 grating, and the RG610 order-cut filter covering 7300–9200 Å. At this redshift, the H α line coincides with a strong night-sky emission line at 8827 Å. To accurately subtract sky emission lines, we utilize the Nod and Shuffle sky subtraction. The signals were 2 pixels binned along the spectral direction. The total integration time was 2640 sec (60 sec \times 2 positions \times 11 cycles \times 2 sequences). The slit position angle was set to the parallactic angle.

3.3 Spectroscopy of the GRB 130427A host galaxy

GRB 130427A is a bright burst at $z = 0.340$ associated with a broad-lined Type Ic SN 2013cq (Xu et al. 2013b; Perley et al. 2014; Levan et al. 2014b). The strong night-sky emission line at 8827 Å overlaps with the [N II] line of the host galaxy at this redshift. Hence accurate subtraction of the sky emission is essential for the spectroscopy of this host galaxy. Although detection of the host galaxy emission lines over the afterglow and the SN are reported by Xu et al. (2013b) and Krühler et al. (2015, hereafter K15), the detection of the [N II] line is marginal in either case, and it is possible that the measured line fluxes are affected by the residual of the strong sky emission line.

The spectroscopic follow up observation of GRB 130427A with Subaru/FOCAS was performed on 2013 May 17 (i.e., ~ 20 days after the burst), under a weather condition with cirrus clouds (PI: N. Kawai). The 0.''8 slit, the 300B grating, and the Y47 filter covering 4700–9000 Å were used. Unfortunately the atmospheric diffraction corrector (ADC) could not be used at the time of the observation. The slit position angle was set to 130° to put both of the center of the host galaxy and the GRB position into the slit. The signals were 2 pixels binned along the spatial direction. The spectroscopy was performed with elevation angles $> 60^\circ$, and atmospheric refraction would be $\lesssim 0.''25$ throughout the wavelength range. The integration time

Table 3. Observations of the GRB host galaxies

target host galaxy	instrument	grating + filter	N&S [†]	Integration [sec]
GRB 060614	GMOS-S	B600	No	1000 × 6
	GMOS-S	R400 + OG515	No	1200 × 8
GRB 090417B	GMOS-N	R831 + RG610	Yes	1320 [‡] × 2
GRB 130427A	GMOS-N	R831 + RG610	Yes	1320 [‡] × 2
GRB 130427A ^{††}	FOCAS	300B + Y47	No	1200 × 8
GRB 111225A	FOCAS	U (imaging)	No	360 × 5
	FOCAS	B (imaging)	No	120 × 5
	FOCAS	V (imaging)	No	120 × 5
	FOCAS	R (imaging)	No	120 × 5
	FOCAS	I (imaging)	No	120 × 5

The observations of the GRB host galaxies we present in this study.

[†] Use of Nod & Shuffle sky subtraction.

[‡] The integration time of 1 Nod & Shuffle sequence consists of 60 sec × 2 positions × 11 cycles.

^{††} TOO, poor weather condition

was 9600 sec. Although the signal-to-noise ratio (S/N) of the obtained spectrum is higher than those previously reported, the significance of the detection of the [N II] line was still low $\sim 4\sigma$ ($\sim 2.5\sigma$ in K15). Furthermore, the [N II] line flux might be affected by the strong sky emission line, as well as in the other observations mentioned above.

We performed further spectroscopy of the GRB 130427A host galaxy with GMOS-North on 2015 March 27, using the Nod and Shuffle sky subtraction to measure the [N II] line flux securely. The setting of the spectrograph and the integration time were the same as that for the observation of the GRB 090417B host galaxy.

3.4 Imaging of the GRB 111225A host galaxy

Thöne & de Ugarte Postigo (2014) reported the redshift of GRB 111225A, $z = 0.297$, in April 2014 (~ 2.3 years after the burst) by analyzing the archival data with an updated software. Thus GRB 111225A was not included in the sample described in section 2 which was compiled in March 2014. We perform imaging observations of the host galaxy of GRB 111225A in U -, B -, V -, R -, and I -band filters with Subaru/FOCAS on 2015 September 22, under a photometric condition. The integration time is 1800 sec for U -band, and 600 sec for each of B -, V -, R -, and I -band. Signals were 2×2 pixels binned. Photometric calibration is performed with respect to Landolt (1992) standard stars in the PG0231+051 field observed in the same night.

4 Emission line measurements

To minimize the effect of stellar absorption features on the line flux measurements, we first subtract stellar spectral energy dis-

tribution (SED) models of the host galaxies from the observed spectra. We perform SED fittings to optical/near-infrared (NIR) broad-band photometries in the literature (figure 1) using the *SEDfit* software package (Sawicki 2012) which utilizes population synthesis models by Bruzual & Charlot (2003). The extinction law by Calzetti et al. (2000) and the initial mass function (IMF) by Chabrier (2003) are assumed. We examine six cases of stellar metallicity: $Z_* = 0.005, 0.02, 0.2, 0.4, 1.0$, and $2.5Z_\odot$, and five cases of star formation history: simple stellar population (SSP), constant star formation, and exponentially decaying star formation with $\tau = 0.2, 1$, and 5 Gyr.

As mentioned in section 3, absolute scale of our spectra is not accurate. Furthermore, it is possible that a fraction light is lost at the slit. In the following discussion, we rescale the observed spectra so that the continuum flux agrees with the best fit SED models. The broad-band photometries, the best fit SED models, and the rescaled spectra are shown in figure 1. The parameters of the best fit stellar SED models are listed in table 4.

There are some archival spectra of the GRB 060614 host galaxy as mentioned in section 3.1, and those by Fynbo et al. (2006) and Gal-Yam et al. (2006) are obtained with GMOS-South using the $1''0$ slit and the R400 grating as well as our R400 spectrum. Although the archival data alone are not deep enough to constrain the metallicity of the host galaxy, we stack them with our R400 spectra to maximize the S/N. The GMOS-South detectors were replaced between the archival observations and ours, the pixel scale remained $\sim 0.7 \text{ \AA}/\text{pix}$ with the R400 grating. The integration time of the archival observations is 1800 sec × 4 and 1200 sec × 4, respectively. We note that the detector replacement improved the efficiency at the wavelength of $H\alpha$ and [N II] at $z = 0.125$ by $\sim 35\%$ ⁸.

We subtract the best fit SED models from the rescaled spectra, and measure emission line fluxes by fitting the lines with Gaussian plus flat continuum models. The residual spectra after the model subtraction and the Gaussian fits are shown in figure 2 and figure 3. Although [O II] line is a doublet, we fit it with a single Gaussian as well as the other lines, because the doublet is not resolved in our spectrum. The obtained emission line fluxes are corrected for the foreground extinction in the Milky Way (MW) using the extinction map by Schlafly & Finkbeiner (2011) and the extinction law by Cardelli et al. (1989), and shown in table 5, together with the emission line fluxes of the other low-redshift GRB host galaxies in the literature.

The continuum component in the spectrum obtained by the FOCAS TOO observation of GRB 130427A is contaminated with the afterglow and the SN (figure 4). Hence we cannot calibrate the flux scale comparing the continuum spectrum with the best fit stellar SED model. Instead, we firstly measure $H\alpha$ flux without the absorption correction, and rescale the FOCAS spectrum so that the absorption uncorrected $H\alpha$ flux agrees with that

⁸ <http://www.gemini.edu/sciops/instruments/gmos/imaging/detector-array>

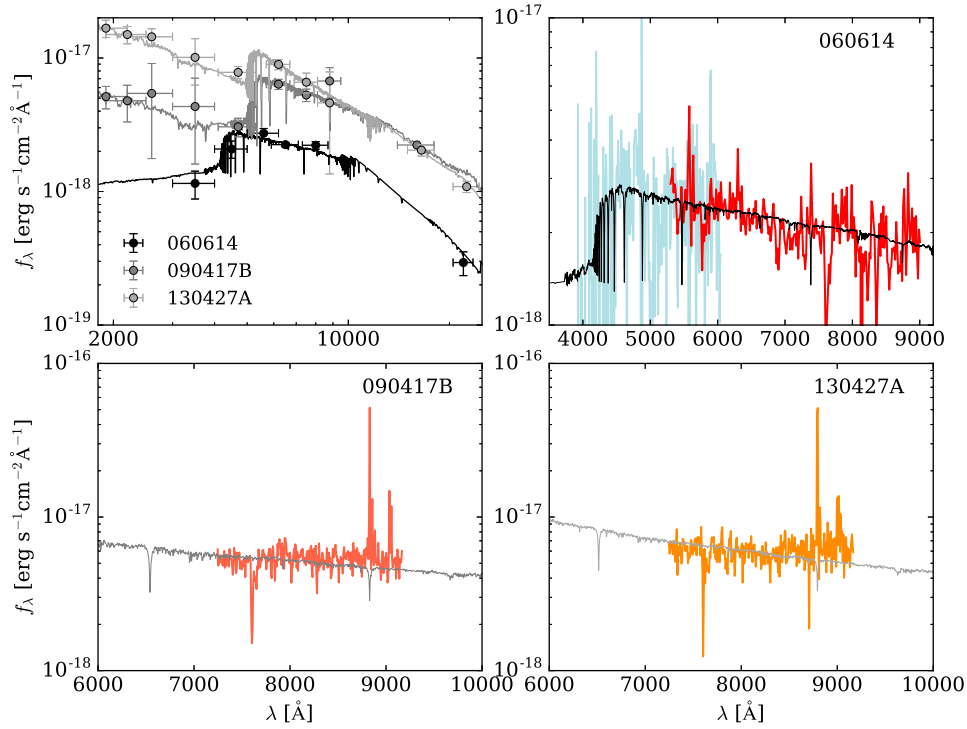


Fig. 1. *Upper left panel:* the optical/NIR broad-band photometries in the literature and the best fit stellar SED models (Bruzual & Charlot 2003). The photometric data are taken from Mangano et al. (2007); Della Valle et al. (2006); Hjorth et al. (2012); Holland et al. (2010); Perley et al. (2013); Perley et al. (2014), and the SDSS SkyServer (<http://skyserver.sdss.org>). *Upper right, lower left, and lower right panels:* the best fit stellar SED models (thin lines) and the GMOS spectra obtained in this study (thick lines) for the host galaxies of GRB 060614, 090417B, and 130427A, respectively. For the host galaxy of GRB 060614, the spectra obtained with the B600, and R400 gratings are shown with light (blue), and dark (red) colored lines, respectively.

Table 4. Results of the host galaxy SED fittings

GRB	$\log_{10} M_*/M_\odot$	Age [Gyr]	$E(B-V)_{\text{SED}}$	Z_*/Z_\odot	star formation history	χ^2
060614	$8.2^{+0.5}_{-0.2}$	$7.8^{+2.4}_{-0.3}$	$0.6^{+0.1}_{-0.6}$	0.005	SSP	6.84
090417B	9.4 ± 0.1	8.8 ± 0.2	0.2 ± 0.1	0.4	$\tau = 0.2$ Gyr	4.49
130427A	9.0 ± 0.1	7.8 ± 0.2	0.2 ± 0.1	0.4	SSP	1.82

The parameters of the best fitting stellar SED models (Bruzual & Charlot 2003) that reproduce the broad-band photometries in the literature (the upper left panel of figure 1). The extinction law by Calzetti et al. (2000) and the IMF by Chabrier (2003) are assumed.

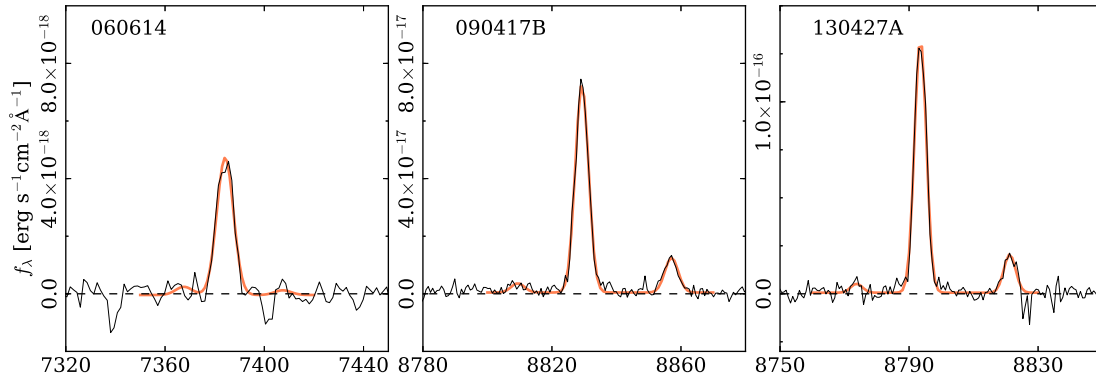


Fig. 2. The $H\alpha$ and $[\text{N II}]$ emission line spectra (the residuals after the model subtraction, thin black lines) of the host galaxies of GRB 060614, 090417B, and 130427A. The thick light-colored (orange) lines are the Gaussian fits to the $[\text{N II}]\lambda 6548$, $H\alpha$, and $[\text{N II}]\lambda 6584$ lines. For the host galaxies of GRB 060614, the spectrum is stacked with the archival data (Fynbo et al. 2006; Gal-Yam et al. 2006).

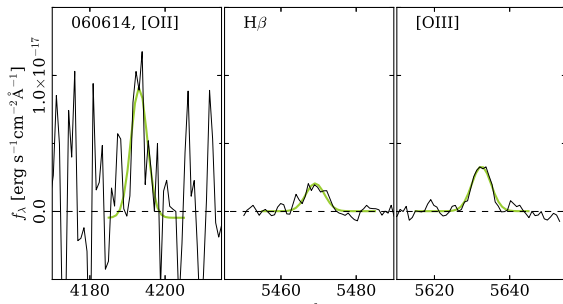


Fig. 3. The same as figure 2, but for the [O II], H β , [O III] lines of the GRB 060614 host galaxy. The spectrum is stacked with the archival data (Fynbo et al. 2006; Gal-Yam et al. 2006) in the wavelength ranges of H β and [O III].

obtained from the GMOS spectrum.

5 Properties of the low-redshift GRB host galaxies

5.1 Metallicity

The emission line fluxes of the host galaxies of all GRBs known at $z \leq 0.41$ as of the end of March 2014 (see section 2) are listed in table 5. With these emission line measurements, we derive metallicity of ionized gas, $12 + \log_{10}(\text{O}/\text{H})$, which would be close to the metallicity of young stars in the galaxies. We utilize both N2 index ($= \log_{10} [\text{N II}]\lambda 6584/\text{H}\alpha$) and R_{23} index ($= ([\text{O II}]\lambda 3727 + [\text{O II}]\lambda 4959 + [\text{O II}]\lambda 5007)/\text{H}\beta$) as indicators of metallicity with the calibration by Kobulnicky & Kewley (2004, KK04) using the same photoionization model (Kewley & Dopita 2002). The solar-metallicity Z_{\odot} corresponds to $12 + \log_{10}(\text{O}/\text{H}) = 8.69$ (Allende Prieto et al. 2001).

In the KK04 calibration, N2 index and the R_{23} index are related to metallicity taking the effect of ionization parameter (q) into account. The q parameter can be estimated from O_{32} index ($= ([\text{O II}]\lambda 4959 + [\text{O II}]\lambda 5007)/[\text{O II}]\lambda 3727$). The metallicity calibration by KK04 suffers from the model uncertainties of ~ 0.1 dex, and hence we consider error of a metallicity measurement to be 0.1 dex when the error propagation from the emission line fluxes is smaller than this value or flux error informations are not available.

The fluxes in table 5 are corrected for the foreground extinction in the MW, but not for the extinction in the host galaxies themselves. To derive metallicity, we correct the line fluxes for the host extinctions, assuming the intrinsic value of the Balmer decrement $\text{H}\alpha/\text{H}\beta = 2.86$ and the extinction law by Calzetti et al. (2000). The positions of the host galaxies on the Baldwin-Phillips-Terlevich (BPT) diagram (Baldwin et al. 1981) with the extinction correction are shown in figure 5. We describe the metallicity determination of each host galaxy in the following. The derived metallicities and the extinctions are listed in table 6.

- **GRB 980425 host galaxy:** the N2 method indicates

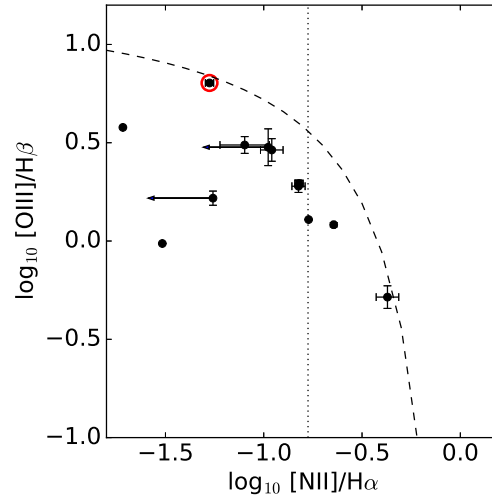


Fig. 5. The low-redshift GRB host galaxies on the BPT diagram. The dashed line represents the empirical demarcation between star-forming galaxies and AGNs (Kauffmann et al. 2003b). The datapoint surrounded by a circle (red) represents the host galaxy of GRB 031203, in which existence of an AGN is suggested (Levesque et al. 2010a). The vertical dotted line represents the [N II]/H α ratio of the host galaxy of GRB 090417B for which the [O III]/H β ratio is not known.

$12 + \log_{10}(\text{O}/\text{H}) = 8.57 \pm 0.10$ and $\log_{10} q = 7.3$, while the R_{23} method does not have any valid solution. The [O III] $\lambda 4959$ flux is not measured in Christensen et al. (2008), and we assume theoretically expected line ratio of [O III] $\lambda 4959$ /[O III] $\lambda 5007 = 1/3$ (e.g., Rosa 1985; Storey & Zeppen 2000). The lack of R_{23} solution generally suggests $12 + \log_{10}(\text{O}/\text{H}) \sim 8.1-8.7$, which is consistent with the N2 solution in this case. We adopt the N2 solution as the best estimate of the metallicity of this host galaxy.

- **GRB 060505 host galaxy:** the N2 method indicates $12 + \log_{10}(\text{O}/\text{H}) = 8.72 \pm 0.10$ and $\log_{10} q = 7.2$ (the best estimate). The R_{23} method does not have valid solution.
- **GRB 031203 host galaxy:** the N2 method indicates $12 + \log_{10}(\text{O}/\text{H}) = 8.75 \pm 0.10$ ($\log_{10} q = 8.6$), and the R_{23} method provides two solutions of $12 + \log_{10}(\text{O}/\text{H}) = 8.48 \pm 0.10$ and 8.32 ± 0.10 (so called upper-/lower-branches, with $\log_{10} q = 8.3$ and 8.2 , respectively).

KK04 calibrated the metallicity indicators in a range of ionization parameter $7.0 \leq \log_{10} q \leq 8.2$, and we need to extrapolate the relation when $\log_{10} q$ is outside of this range. Because the N2 index is sensitive to the ionization parameter, we do not consider the N2 solution for this host galaxy reliable, although the indicated super-solar metallicity suggests the upper-branch solution of the R_{23} method is more likely than the lower-branch solution. Thus we adopt the R_{23} upper-branch solution as the best estimate. The R_{23} upper-

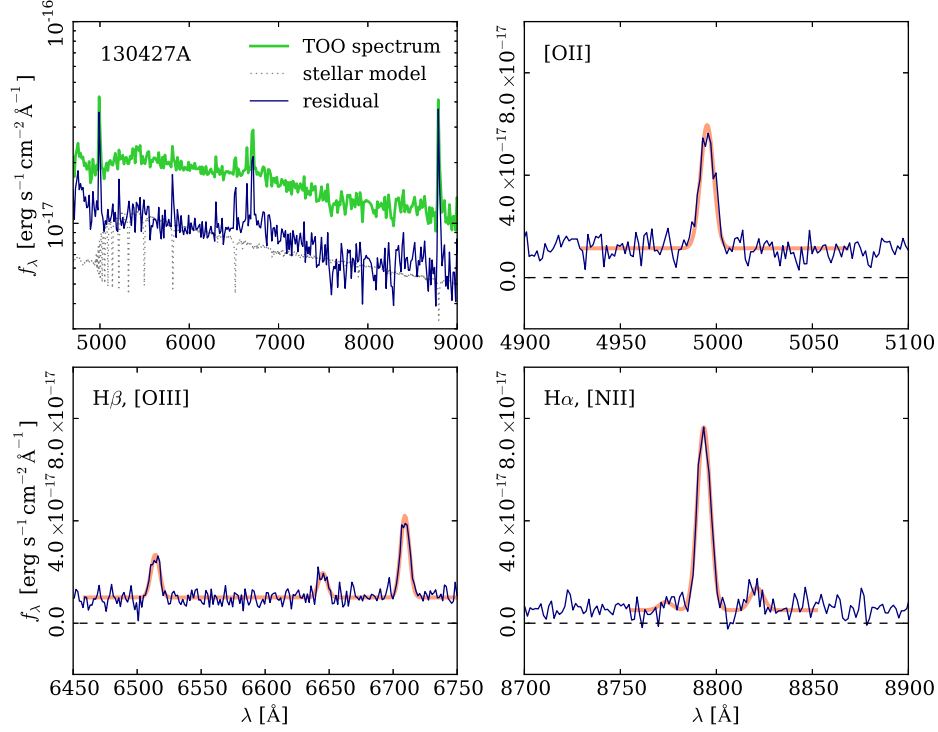


Fig. 4. *Upper left panel:* the spectrum obtained from the TOO observation of GRB 130427A using Subaru/FOCAS, together with the stellar SED model of the host galaxy (the same as that in the top left panel of figure 1), and the residual spectrum after the model subtraction (i.e., the afterglow, the SN, and the emission lines of the host galaxy). *Upper right, lower left, and lower right panels:* the Gaussian plus flat continuum fits to the emission lines in the residual spectrum.

Table 5. Emission line fluxes of the GRB host galaxies at $z \leq 0.41$

GRB	[O II] λ 3727	H β	[O III] λ 4959	[O III] λ 5007	H α	[N II] λ 6584	ref.
980425 [†]	2.40×10^4	4.45×10^3	-	1.29×10^4	1.79×10^4	1.97×10^3	Christensen et al. (2008)
060505	16.8 ± 0.4	4.27 ± 0.03	2.19 ± 0.13	5.17 ± 0.13	21.9 ± 0.09	4.97 ± 0.09	Thöne et al. (2008)
031203	2270 ± 230	2140 ± 40	4520 ± 50	13630 ± 70	6040 ± 30	320 ± 10	Prochaska et al. (2004); Sollerman et al. (2005)
060614	5.60 ± 1.16	1.35 ± 0.10	-	2.23 ± 0.10	4.17 ± 0.09	< 0.28	This work
030329 [‡]	64.8	47.3	57.8	179	151	2.9	Levesque et al. (2010a)
120422	58.0 ± 6.7	12.8 ± 0.4	8.3 ± 0.3	25.1 ± 0.5	53.6 ± 0.5	8.1 ± 0.4	Schulze et al. (2014)
050826 [‡]	70.9	24.5	10.8	31.5	75.7	12.8	Levesque et al. (2010b)
130427A	43.7 ± 1.8 (20.2 ± 2.3)	15.0 ± 1.0 4.8 ± 0.9	8.5 ± 1.0 < 2.2	28.5 ± 1.0 6.5 ± 1.0	62.3 ± 0.9 14.6 ± 1.3	9.36 ± 0.74 1.5 ± 0.6	This work ^{††} K15
090417B	-	-	-	-	38.1 ± 0.6	6.40 ± 0.51	This work
061021	1.6 ± 0.1	0.5 ± 0.1	0.6 ± 0.1	1.5 ± 0.2	1.9 ± 0.1	< 0.26	K15
011121 [‡]	57.97	17.13	16.79	16.64	65.61	2.0	Garnavich et al. (2003); Graham & Fruchter (2013)
120714B	9.8 ± 0.5	2.5 ± 0.2	2.9 ± 0.3	7.7 ± 0.5	7.5 ± 0.3	0.6 ± 0.2	K15
020819B [†]	28.9	18.9	-	9.8	104	44.3	Levesque et al. (2010c)

Fluxes are in units of $10^{-17} \text{ erg s}^{-1} \text{ cm}^{-2}$, and corrected for the foreground extinction in the MW. When the estimated flux is consistent with zero within the 2σ error, we show the 95% upper-limits instead.

[†] The flux errors are $\sim 10\%$.

[‡] Flux error informations are not available.

^{††} The H α and [N II] fluxes are measured from the GMOS spectrum, and the other line fluxes are measured from the FOCAS spectrum.

branch is less sensitive to the ionization parameter than the lower-branch and the N2.

Although the position of this galaxy on the BPT diagram is consistent with being a star forming galaxy (figure 5), Levesque et al. (2010a) showed that the spectrum of this host galaxy is possibly affected by an active galactic nucleus (AGN) investigating more numerous emission line fluxes than examined in the BPT diagram. The high q parameter value also supports the existence of an AGN in the galaxy.

- **GRB 060614 host galaxy:** due to the non-detection of [N II] line, we can put only upper-limit on the N2 index ($N2 < -1.16$). The [O III] λ 4959 line coincides with an strong night-sky emission line, and the flux can not be measured from the observed spectra. Hence we assume the theoretically predicted line ratio of [O III] λ 4959/[O III] λ 5007 = 1/3. The upper- and lower-branch solutions of the R_{23} method are $12 + \log_{10}(\text{O}/\text{H}) = 8.66 \pm 0.10$ and 8.35 ± 0.10 with $\log_{10} q = 7.4$ and 7.3 , respectively. Assuming $\log_{10} q = 7.3$ – 7.4 , the N2 upper-limit indicates $12 + \log_{10}(\text{O}/\text{H}) < 8.4$. Thus we adopt the R_{23} lower-branch solution as the best estimate.
 - **GRB 030329 host galaxy:** the N2, R_{23} upper-branch, and R_{23} lower-branch solutions are $12 + \log_{10}(\text{O}/\text{H}) = 8.07 \pm 0.10$, 8.75 ± 0.10 , and 8.14 ± 0.10 , with $\log_{10} q = 7.8$, 8.2 , and 7.8 , respectively. We adopt the mean of the N2 solution and the R_{23} lower-branch solution.
 - **GRB 120422A host galaxy:** the N2 method indicates $12 + \log_{10}(\text{O}/\text{H}) = 8.65 \pm 0.10$ and $\log_{10} q = 7.3$ (the best estimate). The R_{23} method does not have valid solution.
 - **GRB 050826 host galaxy:** the N2, R_{23} upper-branch, and R_{23} lower-branch solutions are $12 + \log_{10}(\text{O}/\text{H}) = 8.76 \pm 0.10$, 8.86 ± 0.10 , and 8.14 ± 0.10 , with $\log_{10} q = 7.5$, 7.5 , and 7.3 , respectively. We adopt the mean of the N2 solution and the R_{23} upper-branch solution.
 - **GRB 130427A host galaxy:** The N2, R_{23} upper-branch, and R_{23} lower-branch solutions are $12 + \log_{10}(\text{O}/\text{H}) = 8.71 \pm 0.10$, 8.67 ± 0.10 , and 8.33 ± 0.10 , with $\log_{10} q = 7.4$, 7.4 , and 7.3 , respectively. We adopt the mean of the N2 solution and the R_{23} upper-branch solution. However, we note that the FOCAS TOO spectrum from which we measure the emission line fluxes of [O II] λ 3727, H β , and [O III] λ 4959,5007, is obtained without ADC. Hence it is possible that the line fluxes suffer from differential atmospheric refraction.
- To evaluate the effect of this systematic uncertainty, we also examine the independently measured emission line fluxes reported in K15 (shown in table 5). The K15 line fluxes are systematically weaker than those in the GMOS+FOCAS spectra possibly due to larger loss of light at the slit, however we can compare relative flux ratios between the lines.

With the K15 line fluxes, the N2, R_{23} upper-branch, and R_{23} lower-branch solutions are $12 + \log_{10}(\text{O}/\text{H}) = 8.51 \pm 0.11$, $8.70_{-0.14}^{+0.11}$, and $8.34_{-0.12}^{+0.13}$. We note that the detection of the [N II] line is marginal in K15 ($S/N = 2.5$), and it might be affected by the strong sky emission line. Although it is difficult to determine which of the R_{23} solutions is true only with the K15 spectrum, if we adopt the upper-branch solution as suggested by our GMOS spectrum, it agrees well with the estimate from the GMOS+FOCAS spectra.

- **GRB 090417B host galaxy:** the [O II], H β , and [O III] line fluxes are not known. Assuming $7.2 \leq \log_{10} q \leq 7.8$ (the q parameter range covered by the other GRB host galaxies in the sample excluding that of GRB 031203), the N2 method indicates $12 + \log_{10}(\text{O}/\text{H}) = 8.6$ – 8.9 .
- **GRB 061021 host galaxy:** the [N II] line is not detected providing $N2 < -0.86$. The R_{23} upper-branch and lower-branch solutions are $12 + \log_{10}(\text{O}/\text{H}) = 8.43_{-0.15}^{+0.14}$ and $8.51_{-0.19}^{+0.15}$, respectively ($\log_{10} q = 7.5$ in either case). The N2 upper-limit is not deep enough to reject either of the R_{23} solutions. Combining the R_{23} upper-branch and lower-branch solutions, we estimate the metallicity of this host galaxy to be $12 + \log_{10}(\text{O}/\text{H}) = 8.47 \pm 0.19$.
- **GRB 011121 host galaxy:** the N2, R_{23} upper-branch, and R_{23} lower-branch solutions are $12 + \log_{10}(\text{O}/\text{H}) = 8.00 \pm 0.10$, 8.69 ± 0.10 , and 8.33 ± 0.10 , with $\log_{10} q = 7.2$, 7.4 , and 7.2 , respectively. We adopt the mean of the N2 solution and the R_{23} lower-branch solution.
- **GRB 120714B host galaxy:** the N2 method indicates $12 + \log_{10}(\text{O}/\text{H}) = 8.54 \pm 0.11$, although the detection of the [N II] line is marginal. The R_{23} method, which is not affected by the low-S/N of the [N II] line, provides the upper-branch and the lower-branch solutions: $12 + \log_{10}(\text{O}/\text{H}) = 8.50 \pm 0.10$ and 8.43 ± 0.10 , respectively ($\log_{10} q = 7.5$ in either case). We adopt the R_{23} upper-branch solution, which agrees with the N2 solution.
- **GRB 020819B host galaxy:** the N2, R_{23} upper-branch, and R_{23} lower-branch solutions are $12 + \log_{10}(\text{O}/\text{H}) = 8.98 \pm 0.10$, 8.97 ± 0.10 , and 8.07 ± 0.10 , with $\log_{10} q = 7.3$, 7.3 , and 7.0 , respectively. [O III] λ 4959/[O III] λ 5007 = 1/3 is assumed. We adopt the mean of the N2 solution and the R_{23} upper-branch solution.

5.2 Stellar mass and SFR

Stellar mass (M_*) and SFR of the low-redshift GRB host galaxies are listed in table 6. The stellar masses of the host galaxies of GRB 060614, 090417B, and 130427A are derived by the SED fitting assuming the Chabrier IMF as described in section 4, and are broadly consistent with previously reported re-

Table 6. Properties of the host galaxies

GRB	$12+\log_{10}(\text{O}/\text{H})^{ab}$	$\log_{10} q^a$	$E(B-V)_{\text{BD}}^c$	$\log_{10} M_*/M_{\odot}^d$	SFR [$M_{\odot}\text{yr}^{-1}$] ^{de}
980425	8.57	7.3	0.29 ± 0.11	9.22 ± 0.52 [1]	0.3 ± 0.1
060505	8.72	7.2	0.50 ± 0.01	9.64 ± 0.02 [2]	1.1 ± 0.1 [3]
031203 ^f	8.48	8.3	< 0.01	8.26 ± 0.45 [1]	7.5 ± 0.2
060614	8.35	7.3	0.07 ± 0.06	$8.2_{-0.2}^{+0.5}$ [4]	$(9.4_{-1.6}^{+1.9}) \times 10^{-3}$
030329	8.11	7.8	0.1	$7.91_{-0.44}^{+0.12}$ [1]	0.71
120422A	8.65	7.3	0.33 ± 0.03	8.95 ± 0.04 [5]	1.65 ± 0.15
050826	8.81	7.5	0.07	$10.10_{-0.26}^{+0.22}$ [1]	1.17
130427A	8.69	7.4	0.32 ± 0.06	9.0 ± 0.1 [4]	$2.82_{-0.45}^{+0.53}$
	$(8.70_{-0.14}^{+0.11}/8.34_{-0.14}^{+0.11})$	7.3/7.2	0.05 ± 0.15 ⁱ		
090417B	8.6–8.9	7.2–7.8 ^g	-	9.4 ± 0.1 [4]	$1.25_{-0.33}^{+0.45h}$
061021	8.47 ± 0.19	7.5	0.24 ± 0.16	8.5 ± 0.5 [6]	$0.07_{-0.03}^{+0.04}$
011121	8.17	7.2	0.25	9.67 ± 0.17 [7]	2.8
120714B	8.50	7.5	0.04 ± 0.07	-	> 0.2
020819B	8.98	7.3	0.56 ± 0.11	10.65 ± 0.19 [1]	$15.4_{-4.4}^{+6.2}$

^a The best estimates with the KK04 calibration as described in the main text.

^b The estimation errors are $\sim \pm 0.1$ unless otherwise stated.

^c estimated from the Balmer decrement

^d The Chabrier IMF is assumed. The numbers in the square brackets are references as listed below.

^e SFR is derived from the $\text{H}\alpha$ flux in table 5 and $E(B-V)_{\text{BD}}$ in the fourth column unless otherwise stated.

^f Possibly contaminated by an AGN.

^g assumed value

^h The extinction correction is based on the result of the SED fitting: $E(B-V)_{\text{SED}} = 0.2 \pm 0.1$.

ⁱ Derived from the emission line fluxes by K15.

References: 1. Levesque et al. (2010b), 2. Thöne et al. (2008), 3. Castro Cerón et al. (2010), 4. This work, 5. Schulze et al. (2014), 6. Vergani et al. (2015), 7. Küpcü Yoldaş et al. (2007)

sults (Savaglio et al. 2009; Xu et al. 2013b; Perley et al. 2013). We collect M_* measurements of the other host galaxies from the literature. When M_* in the literature is derived assuming an IMF other than the Chabrier IMF, we rescale the mass assuming: $M_{*,\text{Chabrier}} = 0.56M_{*,\text{Salpeter}} = 0.83M_{*,\text{Kroupa}}$ (Chabrier 2003; Brinchmann et al. 2004), for consistency.

We derive SFR of the host galaxies from their extinction corrected $\text{H}\alpha$ fluxes assuming the global Kennicutt-Schmidt law (Kennicutt 1998) and the same scaling factor between the different IMFs as mentioned above. The host galaxy of GRB 060505 is spatially extended over a few $\times 10$ arcsec, and only a part of the emission line fluxes is collected in the slit, and hence we adopt a SFR measured from ultraviolet photometries instead (Castro Cerón et al. 2010). The emission lines of the GRB 120714B host galaxy were detected over the optical afterglow (Fynbo et al. 2012; K15), and the fraction of the host galaxy light in the slit is not known. Hence we consider the obtained SFR for this host galaxy as a lower-limit.

6 Models of the metallicity distribution

6.1 Global properties of star-forming galaxies

To investigate the relation between metallicity and GRB occurrence, we compare the metallicity distribution of the complete sample presented in section 5 with the metallicity distribution of star forming galaxies at similar redshifts. Following Stanek

et al. (2006) and Niino (2011), we compute the metallicity distribution of star forming galaxies using the empirical formulation of stellar mass function [$\phi(M_*)$], M_* -SFR relation (so called “galaxy main-sequence”), and mass-metallicity (M_* - Z) relation of galaxies. In this study, we assume $\phi(M_*)$ by Baldry et al. (2012, blue population), the M_* -SFR relation by Salim et al. (2007, see their equation 11, scatter $\sigma_{\text{MSFR}} = 0.5$ dex) and the M_* - Z relation computed with the KK04 calibration by Kewley & Ellison (2008).

We only consider the mass range $\log_{10} M_* \geq 8.0$, below which the properties of galaxies are not well constrained. This mass limit is also comparable to the lowest-mass GRB host galaxies in the complete sample. M_* and SFR in the formulations are rescaled to be consistent with the Chabrier IMF. The scatter of the M_* - Z relation is largely dependent on M_* in the sense that the scatter is larger at smaller M_* . Here we assume a simple formulation:

$$\sigma_{\text{MZ}} = \begin{cases} -0.05\log_{10} M_* + 0.6 & (\log_{10} M_* < 10.5) \\ 0.075 & (\log_{10} M_* \geq 10.5) \end{cases}, \quad (1)$$

which is broadly consistent with the scatter of the M_* - Z relation discussed in Tremonti et al. (2004).

Although it is suggested that there is a correlation between SFR and metallicity of galaxies with similar stellar masses (Ellison et al. 2008; Mannucci et al. 2010; Lara-López et al. 2010), the observed correlation between SFR and Z correlation is not quantitatively understood affected by sample se-

lections and metallicity calibration methods (e.g. Yates et al. 2012; Niino 2012; Andrews & Martini 2013). Hence we do not consider the correlation in our baseline model, and discuss the effects of the SFR- Z correlation on our results in section 8.1.

6.2 Internal metallicity variation within a galaxy

Observations of some nearby galaxies (MW, the Magellanic Clouds, and M31) show that inter-stellar medium (ISM) in a galaxy is not chemically homogeneous. Hence the metallicity of a GRB progenitor star might be different from the metallicity of the host galaxy which we can measure by follow up spectroscopies.

To examine metallicity variation of star forming regions within a galaxy, we consider observed metallicity distributions of H II regions in nearby galaxies. Although recent integral field unit (IFU) spectroscopies provides us with spatially resolved map of metallicity in some star forming galaxies, the spatial resolution of such observations are still limited to $\gtrsim 100$ pc in most of the cases (e.g., Sánchez et al. 2012). Hence the spectroscopy of individual H II regions (except for giant ones) can be performed only in a few nearby galaxies.

In the upper panel of figure 6, we show the metallicity distributions of H II regions in the MW (solar-neighborhood, Afleverbach et al. 1997), the large/small Magellanic clouds (LMC and SMC, Pagel et al. 1978), and the Andromeda galaxy (M31, Sanders et al. 2012). It is possible that the metallicity estimates of the faint H II regions in the M31 sample by Sanders et al. (2012) have systematic errors (Niino et al. 2015), and hence we consider only H II regions with $H\alpha$ luminosity $> 10^{36.5}$ [erg s $^{-1}$] in the M31 sample. The $H\alpha$ luminosities of the H II regions are taken from Azimlu et al. (2011). See Niino et al. 2015 for the detail of the catalog matching between the samples of Azimlu et al. (2011) and Sanders et al. (2012).

The metallicities of the H II regions can be represented by log-normal distributions but with different median value and dispersion in different galaxies. The median and the scatter of the H II region metallicity distributions in the nearby galaxies [$12+\log_{10}(\text{O}/\text{H})_{\text{gal}}$ and $\sigma_{Z,\text{int}}$] are shown in the lower panel of figure 6. Although the sample number is small, it is seen that the galaxies with the higher median metallicity have larger scatter of the distribution. As a baseline model, we assume a broken linear relation between $12+\log_{10}(\text{O}/\text{H})_{\text{gal}}$ and $\sigma_{Z,\text{int}}$ as shown in the lower panel of figure 6:

$$\sigma_{Z,\text{int}} = \begin{cases} 0.1 & (\log_{10}(\frac{\text{O}}{\text{H}})_{\text{gal}} < -3.7) \\ \frac{2}{3} \times [\log_{10}(\frac{\text{O}}{\text{H}})_{\text{gal}} + 3.85] & (-3.7 \leq \log_{10}(\frac{\text{O}}{\text{H}})_{\text{gal}} < -3.4) \\ 0.3 & -3.4 \leq \log_{10}(\frac{\text{O}}{\text{H}})_{\text{gal}} \end{cases} \quad (2)$$

considering $12+\log_{10}(\text{O}/\text{H})_{\text{gal}}$ equals to the representative metallicity of a galaxy which we obtain by spectroscopically observing the galaxy without spatially resolving it. We also dis-

cuss the results with different $\sigma_{Z,\text{int}}$ formulations in section 8.1.

The metallicities of the nearby H II regions discussed in this section are measured using different metallicity calibration methods than the KK04 calibration which we utilize in this study, and it is known that different metallicity calibrations are often inconsistent with each other (Kewley & Ellison 2008). We consider this possible inconsistency as a part of the uncertainty of $\sigma_{Z,\text{int}}$ which we discuss in section 8.1.

It is broadly agreed that the metallicity decreases as the galactocentric radius increases in many galaxies (so called metallicity gradient, e.g., Shields & Searle 1978). However, we note that a scatter around the gradient at each radius is also significant. The scatter of metallicity at each galactocentric radius can be comparable to (or even larger than) the radial variation (e.g., Sanders et al. 2012), and lowest-metallicity H II regions in a galaxy may reside close to the center of the galaxy.

It should be noted that the scatter of the metallicities in each galaxy may in part result from uncertainties of the metallicity measurements. However, similar variation of metallicity is also found in the MW using stars with ages of ~ 10 Gyr as a tracer of metallicity (Schlesinger et al. 2012). Furthermore, in the M31 H II region sample of Sanders et al. (2012), the weak auroral line [O III] $\lambda 4363$ is detected for four H II regions. With the electron temperature (T_e) method of metallicity measurement using the auroral line (e.g., Garnett 1992), which is not affected by uncertainties of the photoionization models, they showed that the four H II regions have $12+\log_{10}(\text{O}/\text{H}) \sim 8.3\text{--}8.4$. It is generally difficult to detect an auroral line of a high-metallicity H II region, and it is not surprising that the four H II regions with the auroral detections are biased towards low-metallicities. However, the T_e method measurements provides a confirmation that some H II regions in M31 have low-metallicity in reality.

6.3 Metallicity of progenitor stars and GRB production efficiency

We parameterize the relation between GRB production efficiency ($\epsilon_{\text{GRB}} = R_{\text{GRB}}/\text{SFR}$) and metallicity of a population of young stars. As discussed in section 6.2, the metallicity of the stellar population may be different from that of the host galaxy. Here we consider that ϵ_{GRB} is suppressed above a threshold metallicity $(\text{O}/\text{H})_{\text{cut}}$ by a factor of f_{cont} which is not necessarily zero (step function model):

$$\epsilon_{\text{GRB},s} = \begin{cases} \epsilon_{\text{GRB},0} & \text{O}/\text{H} \leq (\text{O}/\text{H})_{\text{cut}} \\ f_{\text{cont}} \epsilon_{\text{GRB},0} & \text{O}/\text{H} > (\text{O}/\text{H})_{\text{cut}} \end{cases} \quad (3)$$

We consider normalized metallicity distribution function (PDF) of GRB host galaxies when we compare the model predictions to the observations, and hence absolute scale of the efficiency (i.e., $\epsilon_{\text{GRB},0}$) is marginalized.

We also consider the cases with the power-law ϵ_{GRB} model:

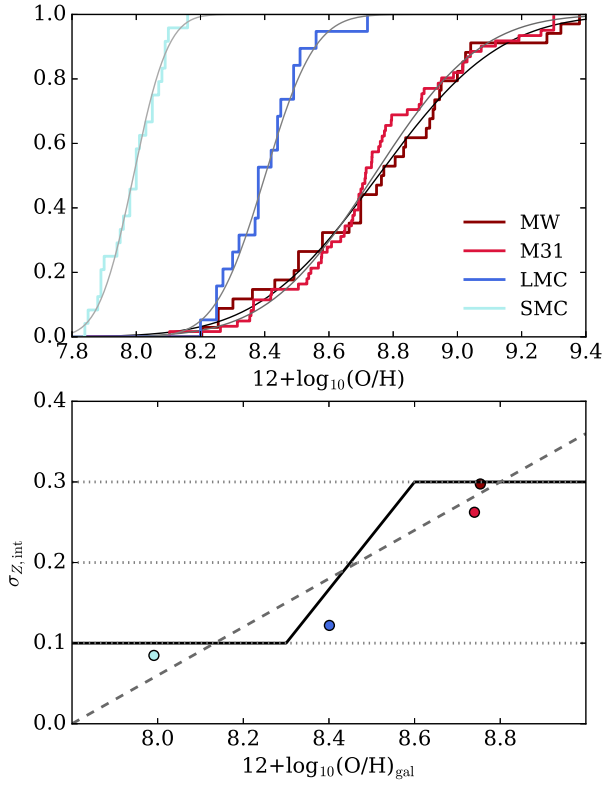


Fig. 6. *Upper panel:* the metallicity distributions of H II regions in the MW (soler-neighbourhood, Afleverbach et al. 1997), the Magellanic clouds (Pagel et al. 1978), and M31 (Sanders et al. 2012, bright objects with $L_{\text{H}\alpha} > 10^{36.5}$ [erg s $^{-1}$]). The best fit log-normal distributions are plotted together. *Lower panel:* the median $[12+\log_{10}(\text{O}/\text{H})_{\text{gal}}]$ and the scatter ($\sigma_{Z,\text{int}}$) of the H II region metallicity distributions in the nearby galaxies. The correlations between $12+\log_{10}(\text{O}/\text{H})_{\text{gal}}$ and $\sigma_{Z,\text{int}}$ which we examine in this study: a broken linear model (solid line), a single linear model (dashed line), and constant models (dotted lines) are plotted together.

$$\epsilon_{\text{GRB},\text{p}} = \begin{cases} \epsilon_{\text{GRB},0} & \text{O}/\text{H} \leq (\text{O}/\text{H})_{\text{cut}} \\ \epsilon_{\text{GRB},0} \times \left[\frac{\text{O}/\text{H}}{(\text{O}/\text{H})_{\text{cut}}}\right]^{\alpha} & \text{O}/\text{H} > (\text{O}/\text{H})_{\text{cut}} \end{cases}, \quad (4)$$

and with the exponential ϵ_{GRB} model:

$$\epsilon_{\text{GRB},\text{e}} = \epsilon_{\text{GRB},0} \times \exp\left(-\left[\frac{\text{O}/\text{H}}{(\text{O}/\text{H})_{\text{cut}}}\right]^{\beta}\right). \quad (5)$$

The schematic picture of the ϵ_{GRB} models is shown in figure 7

GRB rate of a galaxy with a given set of SFR and $12+\log_{10}(\text{O}/\text{H})_{\text{gal}}$ (median metallicity of star forming regions in the galaxy) can be obtained by performing the following integration:

$$R_{\text{GRB},\text{gal}} = \text{SFR} \int \epsilon_{\text{GRB}}(Z) \psi(Z) dZ \equiv \text{SFR} \bar{\epsilon}_{\text{GRB},\text{gal}}, \quad (6)$$

where $\psi(Z)$ is the metallicity distribution of star forming regions in the galaxy which is represented by a log-normal distribution with a median value that corresponds to $12+\log_{10}(\text{O}/\text{H})_{\text{gal}}$ and a log scale scatter $\sigma_{Z,\text{int}}$ (see section 6.2).

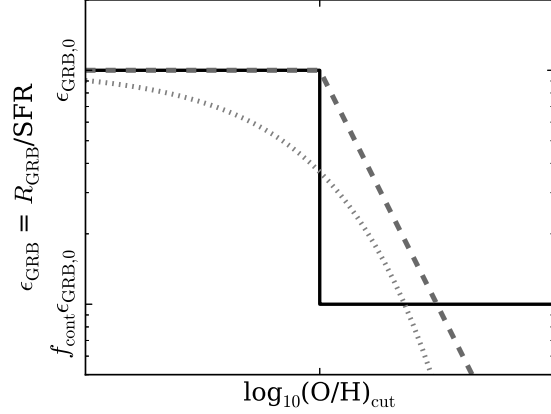


Fig. 7. Schematic picture of the step function (solid, eq. 3), power-law (dashed, eq. 4), and exponential (dotted, eq. 5) models of ϵ_{GRB} as functions of metallicity.

7 Results

Assuming $\phi(M_*)$, the M_* -SFR relation, and the M_* - Z relation, we compute number density of galaxies in the parameter space of M_* , SFR, Z : $\varrho(M_*, \text{SFR}, Z)$ [Mpc $^{-3}$ dex $^{-3}$]. The expected metallicity distribution of GRB host galaxies can be derived integrating $\varrho(M_*, \text{SFR}, Z)$ over M_* and SFR weighted with $R_{\text{GRB},\text{gal}}$ (equation 6).

Each ϵ_{GRB} model discussed in section 6.3 has two free parameters: $[(\text{O}/\text{H})_{\text{cut}}, f_{\text{cont}}]$, $[(\text{O}/\text{H})_{\text{cut}}, \alpha]$, or $[(\text{O}/\text{H})_{\text{cut}}, \beta]$. The parameter $(\text{O}/\text{H})_{\text{cut}}$ determines the cutoff metallicity above which the GRB production efficiency is suppressed, and f_{cont} , α , or β determines the sharpness of the cutoff. We perform parameter fitting of the metallicity distribution models to the observed metallicity distribution of the low-redshift sample (table 6).

The bestfit model distributions are plotted in the upper left panel of figure 8 together with the metallicity distribution of the low-redshift sample. Although the metallicities of the host galaxies of GRB 061021 and 090417B are not precisely constrained (see section 5.1), the uncertainties of these measurements do not significantly affect the overall metallicity distribution of GRB host galaxies. The SFR weighted metallicity distribution predicted from the same $\phi(M_*)$, the M_* -SFR relation, and the M_* - Z relation, which the GRB host galaxies would follow if ϵ_{GRB} is not dependent on metallicity, is also shown together.

The best fit parameters are determined using the Kolmogorov-Smirnov (KS) test as:

step function: $12+\log_{10}(\text{O}/\text{H})_{\text{cut}} = 8.25^{+0.37}_{-0.28}$, $f_{\text{cont}} < 10^{-1.6}$
power-law: $12+\log_{10}(\text{O}/\text{H})_{\text{cut}} = 8.17^{+0.38}_{-0.67}$, $\alpha < -2.0$
exponential: $12+\log_{10}(\text{O}/\text{H})_{\text{cut}} = 8.24^{+0.39}_{-0.74}$, $\beta > 0.6$

where the errors corresponds to the range that the K-S test prob-

ability $P_{\text{KS}} > 0.32$ (i.e., 68% confidence level). The best fitting metallicity distributions with the three different ϵ_{GRB} models are very similar to each other.

The acceptable range of the parameters are shown as contour maps of the P_{KS} in figure 8. The three ϵ_{GRB} models indicates similar threshold metallicities of $12+\log_{10}(\text{O}/\text{H})_{\text{cut}} \sim 8.2$, and the sharper cutoff reproduces the observations better in any of the models. This means that majority of low-redshift GRB host galaxies have higher metallicity than $12+\log_{10}(\text{O}/\text{H})_{\text{cut}}$ above which GRBs cannot be produced. In other words, most low-redshift GRBs takes place in star forming regions whose local metallicity is much lower than the representative value of their host galaxies.

In some cases, GRB positions are spatially resolved from the center (or brightest part) of the host galaxies (e.g., Modjaz et al. 2008). Levesque et al. (2011) has shown that the metallicities at the GRB positions are systematically lower than that of their host galaxies by ~ 0.1 dex, but not necessarily as low as suggested by our results. Niino et al. (2015) pointed out that the actual metallicity of a GRB explosion site cannot be obtained with a spatial resolution $\gtrsim 1$ kpc which is typical of the observations of GRB positions at $z > 0.1$, because the length scale of the ISM metallicity variation is < 1 kpc in nearby galaxies (e.g., Sanders et al. 2012). Our results suggest that the actual metallicity of the GRB explosion sites (or the progenitor star itself) which is buried within the spatial resolution is significantly lower than the kpc scale metallicity currently observed, by up to ~ 0.6 dex.

The model distribution with the step function model of ϵ_{GRB} does not significantly depend on f_{cont} when $\log_{10}f_{\text{cont}} \lesssim -3$, and the distribution with $f_{\text{cont}} = 0.0$ is quite similar to the best fit distribution shown in the upper left panel of figure 8. We also note that, in the limit of $\alpha = -\infty$ ($\beta = \infty$), the power-law (exponential) model of ϵ_{GRB} is identical to the step function model with $f_{\text{cont}} = 0.0$. In the following, we only consider the step function model of ϵ_{GRB} with $f_{\text{cont}} = 0.0$ to examine the predicted properties of low-redshift GRB host galaxies with our models.

The $R_{\text{GRB,gal}}$ weighted distribution of galaxies on the M_* - Z and M_* -SFR parameter planes, predicted using the step function model of ϵ_{GRB} with $12+\log_{10}(\text{O}/\text{H})_{\text{cut}} = 8.25$ and $f_{\text{cont}} = 0.0$, is plotted as contours in figure 9. The SFR weighted model distribution, the assumed M_* - Z relation (Kewley & Ellison 2008), the M_* -SFR relation (Salim et al. 2007), and the observed properties of the low-redshift sample (table 6) are plotted together.

The observed GRB host galaxies construct a sequence which is offset from the M_* - Z relation by 0.1–0.2 dex towards lower-metallicities, as previously noted by Levesque et al. (2010b) with a smaller incomplete sample, except for one remarkable outlier (the host galaxy of GRB 011121). The $R_{\text{GRB,gal}}$

weighted model distribution also shows similar offset on the M_* - Z plane due to the higher $\bar{\epsilon}_{\text{GRB,gal}}$ in galaxies with lower $12+\log_{10}(\text{O}/\text{H})_{\text{gal}}$. Although the offset of the observed GRB host galaxies may be slightly larger than that of the model distribution, this possible contradiction can be resolved by taking the SFR- Z correlation into account as we discuss in section 8.1.

In the M_* -SFR plane, the predicted galaxy distributions with the SFR and $R_{\text{GRB,gal}}$ weightings are offset from the M_* -SFR relation by ~ 0.5 dex ($\sim \sigma_{\text{MSFR}}$, as generally expected when the scatter of a relation is represented by a log-normal distribution). The observed GRB host galaxies are broadly consistent with the predicted offset, although the SFR scatter of the host galaxies with $\log_{10}M_*/M_{\odot} < 9.0$ is large.

The host galaxy of GRB 031203, which might have an AGN, agrees well with the sequence of other GRB host galaxies in the M_* - Z plane, while it is largely offset towards higher-SFR in the M_* -SFR plane. The outlier in the M_* - Z plane, the GRB 011121 host galaxy, does not show any peculiarity in the M_* -SFR plane. The host galaxy with the lowest SFR is that of GRB 060614, which is not associated with a SN and thus possibly a misclassified short GRB. The GRB 060614 host galaxy does not show any peculiarity in the M_* - Z plane.

In figure 10, we compare the step function model of ϵ_{GRB} [$12+\log_{10}(\text{O}/\text{H})_{\text{cut}} = 8.25$, $f_{\text{cont}} = 0.0$] with that convolved over galaxy scale ($\bar{\epsilon}_{\text{GRB,gal}}$) as defined in equation 6. $\bar{\epsilon}_{\text{GRB,gal}}$ steeply declines with increasing metallicity at around $12+\log_{10}(\text{O}/\text{H})_{\text{cut}}$. However, galaxies with $12+\log_{10}(\text{O}/\text{H})_{\text{gal}} > 12+\log_{10}(\text{O}/\text{H})_{\text{cut}}$ have $\bar{\epsilon}_{\text{GRB,gal}} > 0.0$ due to the internal variation of metallicity. The steep decline of $\bar{\epsilon}_{\text{GRB,gal}}$ at $12+\log_{10}(\text{O}/\text{H})_{\text{gal}} \sim 8.2$ is also reported by Graham & Fruchter (2015) based on a GRB host galaxy sample collected from a wider range of redshifts where metallicity measurements of GRB host galaxies are incomplete. We note that $\bar{\epsilon}_{\text{GRB,gal}}(Z)$ likely evolve with redshift because it depends on the properties of galaxies (e.g., $\sigma_{Z,\text{int}}$), unlike $\epsilon_{\text{GRB}}(Z)$ which would be determined by stellar physics.

8 Discussion

8.1 Uncertainties in the models of galaxies

The model predictions of the metallicity distribution depend not only on the ϵ_{GRB} model, but also on the underlying assumptions of the properties of galaxies. In this section, we examine how our results are affected by some galaxy properties which is not well understood, namely the SFR- Z correlation and the variation of metallicity within a galaxy.

To investigate the effect of the SFR- Z correlation, we consider the M_* -SFR- Z relation by Mannucci et al. (2011), which is an extension of the relation by Mannucci et al. (2010) towards lower- M_* . However, the metallicity calibration method used in Mannucci et al. (2011) is different from that used in this study

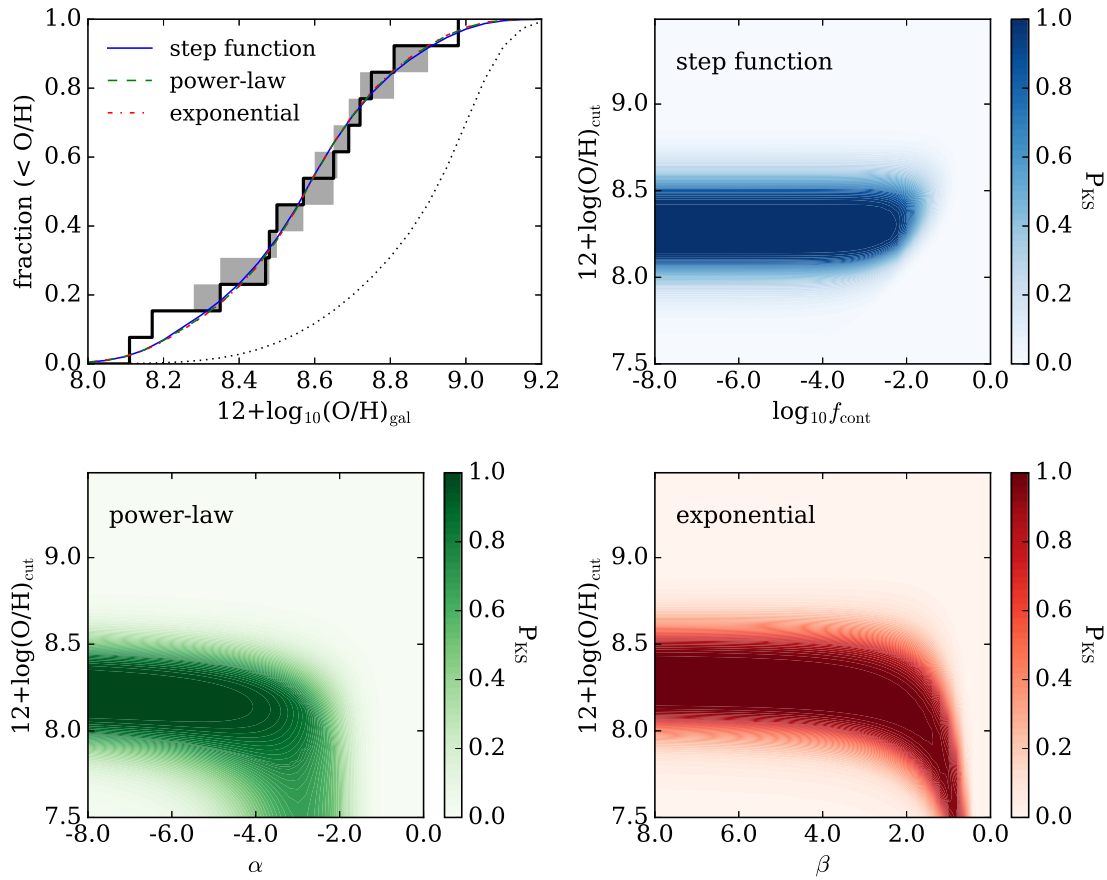


Fig. 8. Upper left panel: the cumulative metallicity distribution of the complete sample of GRB host galaxies at $z \leq 0.41$ (histogram), and the best fit model distributions with the three different ϵ_{GRB} models (solid, dashed, and dot-dashed lines). The SFR weighted metallicity distribution is plotted together (dotted line). The gray shaded region associated with the histogram indicates the error due to the uncertain metallicity measurements of the host galaxies of GRB 061021 and 090417B. Upper right, lower left, and lower right panels: the P_{KS} likelihood distribution as a function of the ϵ_{GRB} model parameters for the step function, power-law, and exponential models, respectively.

(KK04). To examine the effect of the SFR- Z correlation in a consistent metallicity scale, we compute the $\frac{\partial \log_{10}(O/H)}{\partial \log_{10} \text{SFR}}$ gradient of the M_* -SFR- Z relation around the galaxy main-sequence at each M_* . And assume the gradient without changing the M_* - Z relation (Kewley & Ellison 2008), which has been used in the previous sections.

It should be noted that the scatter of the M_* - Z relation at each M_* may partly result from the SFR- Z correlation. Mannucci et al. (2010) showed that the metallicity scatter around the M_* -SFR- Z relation is smaller by 50% than that of the M_* - Z relation. Thus we assume the scatter of the M_* -SFR- Z relation is 50% of that of the M_* - Z relation defined in equation 1.

The resulting P_{KS} contour map and the bestfit metallicity distribution using the step function ϵ_{GRB} model are shown in figure 11 (top panel) and figure 12, respectively. Both the best fit parameters and the goodness of the fit are not significantly different from the case without the M_* - Z relation. This situation is similar with the power-law and exponential models of

ϵ_{GRB} .

The small effect of the SFR- Z correlation on the metallicity distribution is not surprising. The SFR- Z gradient around the galaxy main-sequence is $\frac{\partial \log_{10}(O/H)}{\partial \log_{10} \text{SFR}} = -0.16$ in the low- M_* range ($\log_{10} M_*/M_{\odot} \lesssim 9$) and shallower in higher- M_* ranges. Given that the GRB host galaxies have systematically higher-SFR than the main-sequence by ~ 0.5 dex (section 7), the expected effect of the SFR- Z correlation is $\lesssim 0.08$, which is smaller than the uncertainties of the metallicity measurements.

The SFR and $R_{\text{GRB,gal}}$ weighted model distributions of galaxies on the M_* - Z and M_* -SFR planes, predicted assuming the SFR- Z gradient are shown in figure 13. The ϵ_{GRB} model and the parameters are the same as in figure 9. The SFR weighted galaxy distribution (i.e., no metallicity effect) on the M_* - Z plane is also shifted towards lower-metallicities due to the SFR- Z correlation, but the shift is smaller than that of the $R_{\text{GRB,gal}}$ weighted distribution. Furthermore, the GRB host galaxies have systematically lower- M_* than the typical M_* of the SFR weighted population ($\log_{10} M_*/M_{\odot} \sim 10$), which can-

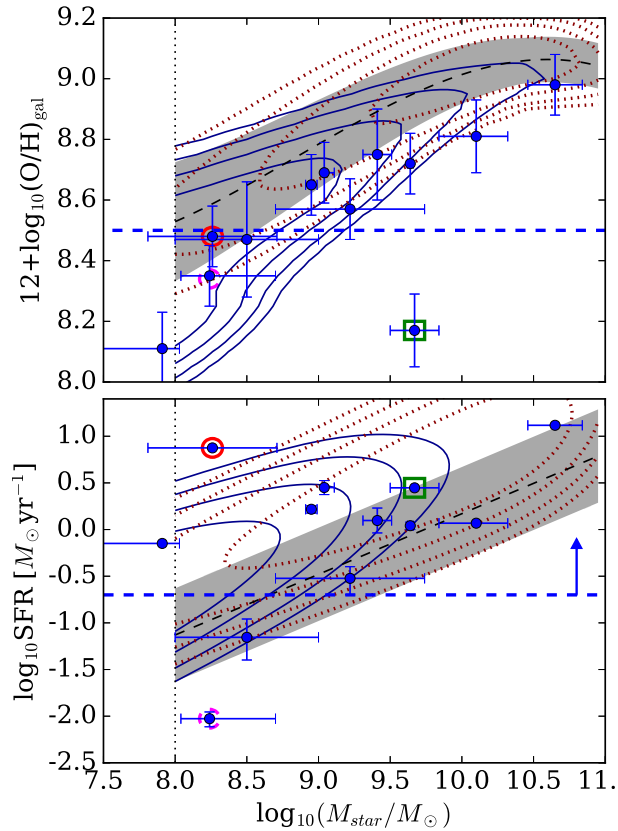


Fig. 9. The predicted and observed distribution of GRB host galaxies on the parameter planes of M_* vs. Z (upper panel), and M_* vs. SFR (lower panel). The solid and dotted contours represent the predicted distributions weighted with the $R_{\text{GRB,gal}}$ and SFR, respectively. The contours are drawn at a logarithmic interval of 0.25 dex from the peaks of the distributions. The horizontal dashed lines represent $12+\log_{10}(\text{O}/\text{H})_{\text{gal}}$ and the lower-limit SFR of the host galaxy of GRB 120714B whose M_* is not known. The dashed lines with gray shaded regions are the M_* - Z relation (Kewley & Ellison 2008) and the M_* -SFR relation (Salim et al. 2007). The shaded regions represent 1σ -scatter of the relations. The following host galaxies are marked with specific symbols: GRB 011121 (square, M_* - Z outlier), 031203 (solid circle, possible AGN, M_* -SFR outlier), 060614 (dashed circle, M_* -SFR outlier). The vertical dotted line indicates the lower-limit of the M_* range which we consider when we predict the metallicity distribution of GRB host galaxies.

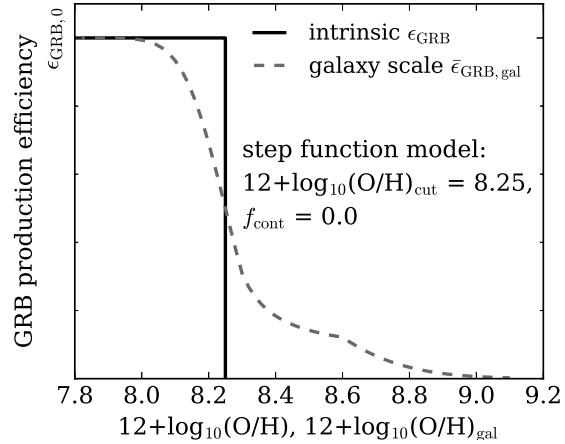


Fig. 10. The GRB production efficiency (ϵ_{GRB}) of a stellar population with a single metallicity [solid line, the step function model with $12+\log_{10}(\text{O}/\text{H})_{\text{cut}} = 8.25$ and $f_{\text{cont}} = 0.0$], and the efficiency convolved over galaxy scale taking the internal variation of metallicity within each galaxy into account (dashed line, see eq. 6).

not be explained solely by the effect of SFR- Z correlation (e.g., Campisi et al. 2011).

Although the SFR- Z correlation does not significantly affect the overall metallicity distribution of the GRB host galaxies as mentioned above, the predicted number of GRB host galaxies above the M_* - Z relation is significantly reduced (figure 13, top panel). This improves the consistency between the predicted and observed distributions of GRB host galaxies on the M_* - Z plane compared with the case without the SFR- Z correlation (figure 9).

As mentioned in section 6.2, the detailed investigation of the internal ISM metallicity variation is performed only for a small number of nearby galaxies. Therefore, $\sigma_{Z,\text{int}}$ of general star forming galaxies and its correlation with other galaxy properties are highly uncertain. To investigate how our results depend on the assumed $\sigma_{Z,\text{int}}$, we perform the parameter fittings assuming other $\sigma_{Z,\text{int}}$ formulations than the baseline model. Here we consider a single linear relation between $12+\log_{10}(\text{O}/\text{H})_{\text{gal}}$ and $\sigma_{Z,\text{int}}$, and also constant $\sigma_{Z,\text{int}}$ of 0.1, 0.2, and 0.3 dex (figure 6, bottom panel). However, it should be noted that the constant $\sigma_{Z,\text{int}}$ is disfavored by observations.

The P_{KS} contour maps and the predicted metallicity distributions are shown in figure 11 and figure 12 for the cases with the single linear relation, and the constant $\sigma_{Z,\text{int}}$ of 0.1 and 0.3 dex. The single linear relation between $12+\log_{10}(\text{O}/\text{H})_{\text{gal}}$ and $\sigma_{Z,\text{int}}$ slightly overpredicts the contribution of high-metallicity galaxies to the GRB production even with the best fit parameters, due to the large $\sigma_{Z,\text{int}}$ of galaxies with $12+\log_{10}(\text{O}/\text{H})_{\text{gal}} > 8.8$. However, the overprediction is not statistically significant ($P_{KS} = 0.38$). The best fit parameters are similar to the case with the baseline model.

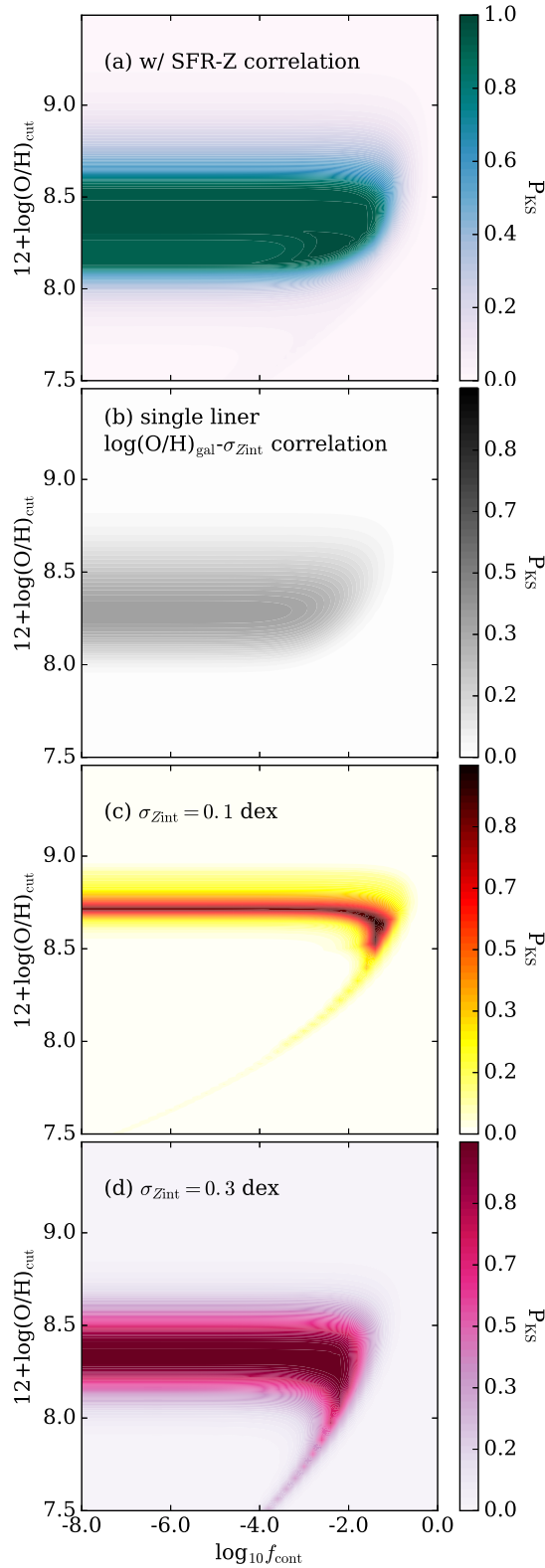


Fig. 11. Same as the upper right panel of figure 8, but with different assumptions of the properties of galaxies. The step function model of ϵ_{GRB} is utilized. (a): the correlation between SFR and $\log_{10}(\text{O}/\text{H})$ is incorporated. (b): $\sigma_{Z,\text{int}}$ is linearly correlated with $12+\log_{10}(\text{O}/\text{H})_{\text{gal}}$. (c) and (d): $\sigma_{Z,\text{int}}$ is a constant value (0.1 and 0.3 dex, respectively).

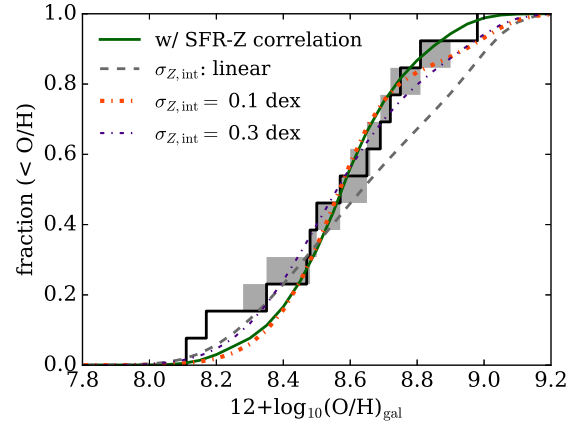


Fig. 12. Same as the upper left panel of figure 8, but with different assumptions of the properties of galaxies. The step function model of ϵ_{GRB} is utilized. The plotted models are the same as those investigated in figure 11.

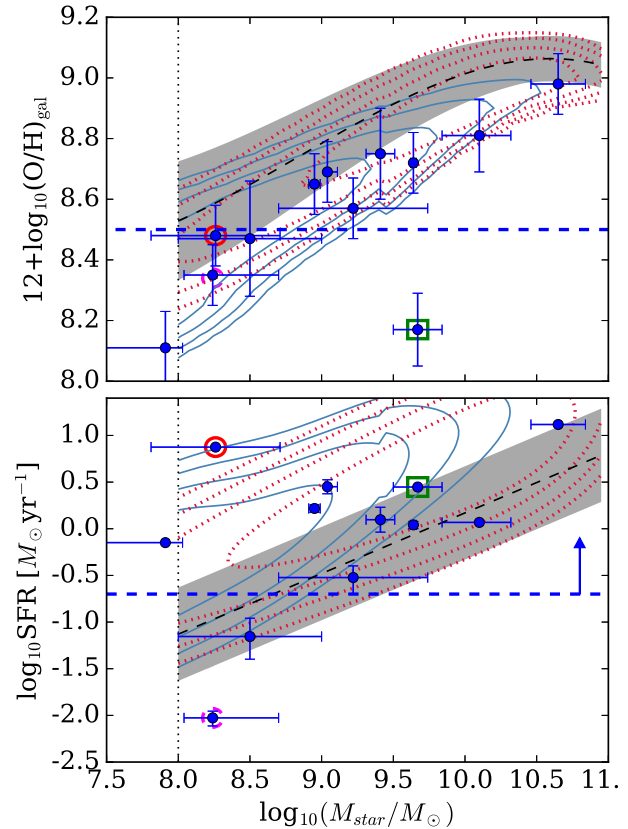


Fig. 13. Same as figure 9, but with the SFR-Z correlation. The anomalies in the contour lines at $\log_{10} M_*/M_\odot \sim 9.5$ result from a discontinuity of the M_* -SFR-Z relation by Mannucci et al. (2011).

When $\sigma_{Z,\text{int}} = 0.1$ dex independently of $12+\log_{10}(\text{O}/\text{H})_{\text{gal}}$, the preferred cutoff metallicity is $12+\log_{10}(\text{O}/\text{H})_{\text{cut}} = 8.64_{-0.25}^{+0.15}$ ($\sim Z_{\odot}$). The cutoff metallicity around Z_{\odot} is consistent with the results of previous studies in which the internal metallicity variation within galaxies is not explicitly treated (e.g., Wolf & Podsiadlowski 2007; Kocevski et al. 2009; Perley et al. 2016b; Japelj et al. 2016). Even in this case, high ϵ_{GRB} in high-metallicity stellar population is disfavored ($f_{\text{cont}} < 0.1$).

When $\sigma_{Z,\text{int}} = 0.3$ dex, the cutoff metallicity is $12+\log_{10}(\text{O}/\text{H})_{\text{cut}} = 8.22_{-0.71}^{+0.38}$, which is close to the results with the baseline model. The results with the constant $\sigma_{Z,\text{int}} = 0.2$ dex are similar with those with 0.1, and 0.3 dex, but with $12+\log_{10}(\text{O}/\text{H})_{\text{gal}} = 8.47_{-0.40}^{+0.26}$.

8.2 Possible subpopulations

Some of the low-redshift GRBs are less energetic than typical GRBs that are observed up to higher-redshifts (hereafter classical GRBs), and possibly are different kind of phenomena. These bursts, so called low-luminosity GRBs, have isotropic equivalent gamma-ray energy $E_{\text{iso}} \lesssim 10^{50}$ [erg] (e.g., Bromberg et al. 2011; Nakar 2015). Stanek et al. (2006) have shown that E_{iso} of a GRB might be dependent on the metallicity of its host galaxy based on observations of the host galaxies of 5 GRBs/XRFs at redshifts ≤ 0.25 , while later studies (Levesque et al. 2010d; Japelj et al. 2016) have shown that there is no significant correlation between them with a larger sample from wider range of redshifts (up to $z = 1$).

Because low-luminosity GRBs can be detected only at low-redshifts $\lesssim 0.3$, the comparison of the host galaxies and low-luminosity GRBs and with those of classical GRBs at $z \sim 1$ might be affected by evolution of galaxy populations over the redshifts. Thus it is interesting to revisit the correlation between E_{iso} and host metallicity with our sample limited to low-redshifts but much larger than that of Stanek et al. (2006). E_{iso} of the low-redshift GRBs and $12+\log_{10}(\text{O}/\text{H})_{\text{gal}}$ are shown in the left panel of figure 14.

E_{iso} is continuously distributed without significant gap over $\sim 10^{48}-10^{54}$ [erg]. No significant correlation between E_{iso} and $12+\log_{10}(\text{O}/\text{H})_{\text{gal}}$ is found (correlation coefficient is 0.08). Thus, in terms of the $E_{\text{iso}}-Z$ correlation, we find no evidence that classical and low-luminosity GRBs are different kind of phenomena.

GRB 060505 and 060614 are widely known as GRBs which are not associated with SNe (Gehrels et al. 2006; Fynbo et al. 2006; Della Valle et al. 2006; Gal-Yam et al. 2006), and it is possible that they are actually short GRBs that do not result from core-collapse of massive stars despite their long duration > 2 sec (e.g., Zhang et al. 2009). These bursts are marked with circles in figure 14. The host metallicities and E_{iso} of GRB 060505 and 060614 are typical of low-redshift GRBs in our sample.

8.3 Sampling biases

In this study, we have compiled the complete list of the host metallicity measurements of all GRBs known at $z \leq 0.41$ to get rid of the reporting bias from our sample. However, the fraction of GRBs with spectroscopic redshifts are $\sim 30\%$ even in recent observations (e.g., Perley et al. 2016a), and hence we may suffer from the redshift determination bias by collecting GRBs with known redshifts.

One possible source of the redshift determination bias is “dark” GRBs (e.g., Jakobsson et al. 2004; Greiner et al. 2011). A “dark” GRB is a GRB with a fainter optical afterglow than expected from its X-ray spectrum. Roughly 1/3 of GRBs are “dark”, and most of them ($\sim 80\%$) result from dust extinction, while some may result from absorption by neutral hydrogen in inter-galactic medium at high-redshifts (Cenko et al. 2009; Zheng et al. 2009; Greiner et al. 2011). Redshift determination of GRBs largely relies on optical spectroscopy of afterglows, and it is difficult to determine redshifts of “dark” GRBs. Thus a sample of GRB host galaxy with known redshifts may be biased against dusty galaxies which may tend to have higher-metallicity.

However, at low-redshifts, detection of a GRB host galaxy is not quite challenging in most of the cases. Assuming the stellar-mass to luminosity ratio derived by Kauffmann et al. (2003a), a galaxy with $M_{\star} = 10^9 M_{\odot}$, which is typical of the low-redshift GRB host galaxies, would be observed with r -band magnitude ~ 24 at $z = 0.3$. Once the host galaxy of a GRB is detected, X-ray afterglow localization by *Swift*/XRT with typical precision of a few arcseconds, which is available for $\sim 80\%$ of the *Swift*/BAT-detected GRBs, can associate the GRB to the host galaxy with a certain level of confidence (Perley et al. 2013). And the redshift can be determined using emission lines of the host galaxy.

In reality, many redshifts of the low-redshift GRBs are determined by the emission lines of the host galaxies (table 2), including those of two “dark” GRBs, 020819B and 090417B (marked with squares in figure 14). Redshift determination by host emission lines is rarely available at higher redshifts. The fraction of the GRBs whose redshifts are determined only by the host emission lines in the low-redshift sample (8/13) is naively comparable to the fraction of GRBs without known redshifts in the *Swift*/BAT-detected GRBs. Thus the bias against GRBs in dusty environment is not necessarily effective at low-redshifts.

Because *Swift* dramatically improved the success rate of host identification and redshift determination of GRBs, the GRBs with known redshifts that have occurred before the launch of *Swift* may suffer the sampling biases more than GRBs detected by *Swift*. In figure 14, GRBs that have occurred before and after the launch of *Swift* is shown with different symbols. We note that all GRBs occurred after the launch of *Swift* in our sample are *Swift*/BAT-detected. There is no systematic difference in

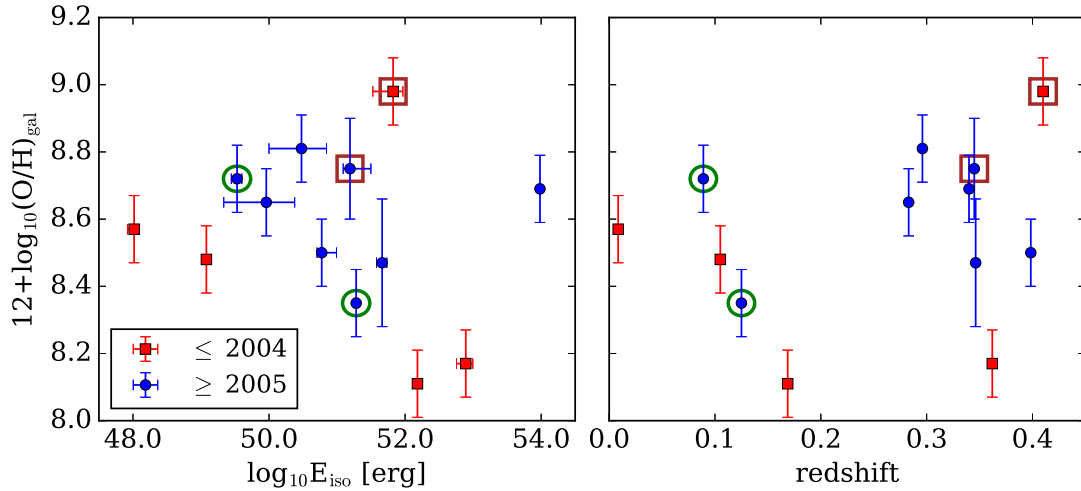


Fig. 14. The E_{iso} vs. host metallicity plot (*left panel*) and the redshift vs. host metallicity plot (*right panel*) of the low-redshift GRBs. GRBs that occurred before and after the launch of the *Swift* satellite (2004) are shown with different symbols (red squares and blue circles, respectively). The data points surrounded by (green) circles represent GRBs without SN associations (GRB 060505 and 060614). The data points surrounded by (brown) squares represent “dark” GRBs (GRB 020819B and 090417B).

E_{iso} , redshifts, and host metallicities of GRBs between the different epochs within the redshift range considered here.

It is possible that GRBs whose redshifts are determined with the emission lines of their host galaxies are biased against GRBs that occurred in galaxies with weak emission line fluxes. Emission line luminosities of a galaxy is largely dependent on SFR in the galaxy, which correlates with M_* and $12 + \log_{10}(\text{O}/\text{H})_{\text{gal}}$, in the sense that galaxies with higher M_* and $12 + \log_{10}(\text{O}/\text{H})_{\text{gal}}$ have more luminous emission lines. Hence GRBs that occurred in very low-metallicity host galaxies might be systematically missed in the low-redshift sample, especially at higher-end of the redshift range where detection of weak emission lines are difficult. However, such redshift dependent metallicity bias is not seen in our sample (the right panel of figure 14, correlation coefficient is 0.23).

On the other hand, it is also true that redshift determination of a GRB has failed (partly) due to the weak emission line of the host galaxy. As mentioned in section 3, the redshift of GRB 111225A has not been determined until Thöne & de Ugarte Postigo (2014) reports detections of weak emission lines over the afterglow together with a marginal absorption line using an updated analysis tool.

Photometries of the host galaxy of GRB 111225A from our imaging observations with Subaru/FOCAS (section 3.4) are listed in table 7. Although the relatively large foreground extinction may be the cause of the faintness of the GRB 111225A host galaxy [$E(B - V) = 0.23$, Schlafly & Finkbeiner 2011], galaxies with $M_* \sim 5 \times 10^8 M_\odot$ would have similar magnitudes at the same redshift ($z = 0.297$) without foreground extinctions (Kauffmann et al. 2003a), and also similar emission line fluxes if the equivalent widths are the same. The failure of the redshift

determination in the immediate follow up observations after the burst suggests that GRB host galaxies with $M_* \lesssim 10^8 M_\odot$ might be missed in redshift selected samples. Thus the metallicity distribution of the overall population of GRB host galaxies at low-redshifts may extend towards lower-metallicities than discussed in this study.

In addition to GRB 111225A, there are two GRBs that occurred before the end of March 2014, but was reported to be at low-redshifts after the date. Rossi et al. (2014) suggests GRB 050219 might have occurred in an early-type galaxy with little star formation at $z = 0.211$, although the chance of coincidence $\sim 0.8\%$ is not negligibly low. Because GRBs result from death of massive stars, the association of GRB 050219 with an early-type galaxy is surprising, however it is not strictly prohibited because early-type galaxies can harbour small amount of star formation (e.g., Morganti et al. 2006). If the association is true, GRB 050219 is the another case in which the redshift determination was initially not successful due to the lack of strong emission lines in the spectrum of the host galaxy, although the large offset of the burst position from the host galaxy ($\sim 2''$) also hinders the host identification and the redshift determination of this burst.

Stanway et al. (2015) performed spectroscopy of the GRB 080517 host galaxy, and measured the redshift of $z = 0.089$. The host galaxy of GRB 080517 is a bright star burst galaxy with r -band magnitude 17.73. The lack of earlier follow up observations may be due to the proximity of the Sun ($< 50^\circ$), and unrelated to the properties of the host galaxies.

It is also interesting to compare the expected rate of low-redshift GRBs to the actual finding rate to evaluate the success rate of identifying low-redshift GRBs. Based on the largest un-

Table 7. Photometries of the host galaxy of GRB 111225A

U	B	V	R	I
$> 24.5^\dagger$	25.3 ± 0.2	24.5 ± 0.1	24.7 ± 0.1	24.1 ± 0.1

Magnitudes are in the AB system, and not corrected for the foreground extinction in the MW [$E(B - V) = 0.23$, Schlafly & Finkbeiner 2011].

† 2σ -limit.

biased GRB survey to date (SHOALS), Perley et al. (2016a) estimated the event rate density of bright GRBs with $E_{\text{iso}} > 10^{51}$ [erg] at $z < 0.5$ to be $0.2_{-0.1}^{+0.3}$ [$\text{yr}^{-1}\text{Mpc}^{-3}$]. Considering the field of view of *Swift*/BAT (1.4 steradian) and the operation time until the end of March 2014 (9.3 years since December 2004), the expected number of bright GRBs detected by *Swift*/BAT at $z \leq 0.41$ in the time period is $3.4_{-1.7}^{+5.1}$. On the other hand, the number of *Swift*/BAT-detected GRBs with $E_{\text{iso}} > 10^{51}$ [erg] in our sample is 4 (figure 14), which suggests that the success rate of redshift determination is higher at low-redshifts compared with that of the overall population of GRBs, although the estimation of the GRB rate density is still uncertain. The faint end of the GRB luminosity function is still controversial affected by sample selections and model assumptions (e.g., Schmidt 2001; Wanderman & Piran 2010; Salvaterra et al. 2012). Hence it is difficult to estimate the actual rate and evaluate the redshift success rate of low-luminosity GRBs.

9 Conclusions

We have presented the complete metallicity measurements of the host galaxies of all long GRBs whose redshifts are spectroscopically determined to be ≤ 0.41 before the end of March 2014, including the newly obtained emission line fluxes of the host galaxies of GRB 060614, 090417B, and 130427A. The low-redshift sample of GRB host galaxies with complete metallicity measurements is essential to study the nature of GRB progenitor in some aspects: 1) the high success rate of redshift determinations and host identifications, 2) the reporting bias can be eliminated by completing the metallicity measurements, and 3) a wealth of comparison sample is available.

We have compared the metallicity distribution of the low-redshift sample with the predictions from the empirical formulations of the properties of low-redshift galaxies. To predict the metallicity distribution, we adopted models of GRB efficiency ($\epsilon_{\text{GRB}} = R_{\text{GRB}}/\text{SFR}$) as functions of metallicity. The metallicity of the progenitor stars considered here is not necessarily identical to that of its host galaxy. Instead, we considered the metallicity variation within each galaxy motivated by the observations of H II regions in nearby galaxies.

The three different formulations of ϵ_{GRB} , namely the step function, power-law, and exponential models are examined. Each of the three ϵ_{GRB} models has two free parameters that can be used to fit the metallicity distribution of the host

galaxies. In either case, ϵ_{GRB} function with a sharp cut-off around $12+\log_{10}(\text{O}/\text{H})_{\text{cut}} \sim 8.2$ reproduces the metallicity distribution of the low-redshift sample best, in agreement with the predictions of the stellar evolution models (Yoon & Langer 2005; Hirschi et al. 2005; Woosley & Heger 2006). ϵ_{GRB} models with moderate or weak metallicity dependence [$\epsilon_{\text{GRB}}(Z_{\odot})/\epsilon_{\text{GRB}}(0.1Z_{\odot}) > 0.1$] are disfavored, although the statistical significance of the current constraints is still low.

This result is in contrast to the results of some previous studies which suggest that the cutoff metallicity is $12+\log_{10}(\text{O}/\text{H})_{\text{cut}} \sim 8.7$ ($\sim Z_{\odot}$, e.g., Wolf & Podsiadlowski 2007; Kocevski et al. 2009; Perley et al. 2016b; Japelj et al. 2016). This is because we take the internal variation of metallicity within each galaxy into account. Our galaxy models also indicate the cutoff metallicity around $\sim Z_{\odot}$, when the internal metallicity variation is assumed to be small (0.1 dex) in any galaxy.

The effect of the correlation between SFR and metallicity of galaxies on the predicted metallicity distribution is smaller than the uncertainty of metallicity measurement. However, it may improve the agreement of the predicted and observed distribution of the GRB host galaxies on the parameter plane of M_{\star} versus Z .

The relation between the nature of GRB progenitor stars and the observable properties of their host galaxy depends on the internal and global properties of galaxies. Better understanding on the general population of galaxies at each redshift is essential to obtain more robust constraints on the properties of GRB progenitors, in addition to gathering larger less biased sample of GRB host galaxies.

Because we collected GRBs with known redshifts (≤ 0.41) in this study, it is possible that the sample of the host galaxies is biased for a kind of galaxy population in which GRB redshift determination is easy (e.g., galaxies with smaller dust content), although the GRB redshift determination is generally easier at lower-redshifts. However, the number of low-redshift GRBs in our sample is close to the number expected from the latest unbiased surveys, suggesting a high success rate of redshift determinations at low-redshifts, although the statistical error is still large. Furthermore, the obtained metallicities do not show significant systematic trend with respect to burst energy (E_{iso}) and redshift. Thus there is no sign that the low-redshift sample of the GRB host galaxies is biased compared to the actual population of GRB host galaxies, although the tests are not robust yet.

On the other hand, the failure of the redshift determination of GRB 111225A in the immediate follow up observations after the burst suggests that faint (and thus low-metallicity) host galaxies might be systematically missed in the redshift selected sample. The more precise estimation of the low-redshift GRB rate will enable us to evaluate sampling biases in the redshift

selected sample robustly.

We thank Gemini and Subaru observatory staffs for their kind support for the observations. YN is supported by the Research Fellowship for Young Scientists from the Japan Society for the Promotion of Science (JSPS). This research has made use of the GHostS database (www.grbhosts.org), which is partly funded by Spitzer/NASA grant RSA Agreement No. 1287913. Thanks are also due to Nathaniel R. Butler, Jochen Greiner, and Daniel A. Perley, for producing the useful online databases.

References

- Afflerbach, A., Churchwell, E., & Werner, M. W. 1997, *ApJ*, 478, 190
- Allende Prieto, C., Lambert, D. L., & Asplund, M. 2001, *ApJL*, 556, L63
- Andrews, B. H., & Martini, P. 2013, *ApJ*, 765, 140
- Azimlu, M., Marciniak, R., & Barmby, P. 2011, *AJ*, 142, 139
- Baldry, I. K., et al. 2012, *MNRAS*, 421, 621
- Baldwin, J. A., Phillips, M. M., & Terlevich, R. 1981, *PASP*, 93, 5
- Berger, E., & Fox, D. B. 2009, *GRB Coordinates Network*, 9156
- Brinchmann, J., Charlot, S., White, S. D. M., Tremonti, C., Kauffmann, G., Heckman, T., & Brinkmann, J. 2004, *MNRAS*, 351, 1151
- Bromberg, O., Nakar, E., & Piran, T. 2011, *ApJL*, 739, L55
- Bromberg, O., Nakar, E., Piran, T., & Sari, R. 2013, *ApJ*, 764, 179
- Bruzual, G., & Charlot, S. 2003, *MNRAS*, 344, 1000
- Butler, N. R., Kocevski, D., Bloom, J. S., & Curtis, J. L. 2007, *ApJ*, 671, 656
- Calzetti, D., Armus, L., Bohlin, R. C., Kinney, A. L., Koornneef, J., & Storchi-Bergmann, T. 2000, *ApJ*, 533, 682
- Campisi, M. A., Tapparello, C., Salvaterra, R., Mannucci, F., & Colpi, M. 2011, *MNRAS*, 417, 1013
- Cardelli, J. A., Clayton, G. C., & Mathis, J. S. 1989, *ApJ*, 345, 245
- Castro Cerón, J. M., Michałowski, M. J., Hjorth, J., Malesani, D., Gorosabel, J., Watson, D., Fynbo, J. P. U., & Morales Calderón, M. 2010, *ApJ*, 721, 1919
- Cenko, S. B., et al. 2009, *ApJ*, 693, 1484
- Chabrier, G. 2003, *PASP*, 115, 763
- Christensen, L., Vreeswijk, P. M., Sollerman, J., Thöne, C. C., Le Floch, E., & Wiersema, K. 2008, *A&A*, 490, 45
- Della Valle, M., et al. 2006, *Nature*, 444, 1050
- Ellison, S. L., Patton, D. R., Simard, L., & McConnell, A. W. 2008, *ApJL*, 672, L107
- Fugazza, D., et al. 2006, *GRB Coordinates Network*, 5276
- Fynbo, J. P. U., de Ugarte Postigo, A., D'Elia, V., Xu, D., & Malesani, D. 2012, *GRB Coordinates Network*, 13477
- Fynbo, J. P. U., et al. 2006, *Nature*, 444, 1047
- . 2009, *ApJS*, 185, 526
- Gal-Yam, A., et al. 2006, *Nature*, 444, 1053
- Garnavich, P. M., et al. 2003, *ApJ*, 582, 924
- Garnett, D. R. 1992, *AJ*, 103, 1330
- Gehrels, N., et al. 2006, *Nature*, 444, 1044
- Graham, J. F., & Fruchter, A. S. 2013, *ApJ*, 774, 119
- . 2015, *ArXiv e-prints*
- Greiner, J., Peimbert, M., Esteban, C., Kaufer, A., Jaunsen, A., Smoke, J., Klose, S., & Reimer, O. 2003, *GRB Coordinates Network*, 2020
- Greiner, J., et al. 2011, *A&A*, 526, A30
- Halpern, J. P., & Mirabal, N. 2006, *GRB Coordinates Network*, 5982
- Hirschi, R., Meynet, G., & Maeder, A. 2005, *A&A*, 443, 581
- Hjorth, J., et al. 2012, *ApJ*, 756, 187
- Holland, S. T., et al. 2010, *ApJ*, 717, 223
- Hook, I. M., Jørgensen, I., Allington-Smith, J. R., Davies, R. L., Metcalfe, N., Murowinski, R. G., & Crampton, D. 2004, *PASP*, 116, 425
- Infante, L., Garnavich, P. M., Stanek, K. Z., & Wyrzykowski, L. 2001, *GRB Coordinates Network*, 1152
- Jakobsson, P., Hjorth, J., Fynbo, J. P. U., Watson, D., Pedersen, K., Björnsson, G., & Gorosabel, J. 2004, *ApJL*, 617, L21
- Jakobsson, P., et al. 2005, *ApJ*, 629, 45
- Japelj, J., et al. 2016, *ArXiv e-prints*
- Kashikawa, N., et al. 2002, *PASJ*, 54, 819
- Kauffmann, G., et al. 2003a, *MNRAS*, 341, 33
- . 2003b, *MNRAS*, 346, 1055
- Kennicutt, Jr., R. C. 1998, *ApJ*, 498, 541
- Kewley, L. J., & Dopita, M. A. 2002, *ApJS*, 142, 35
- Kewley, L. J., Dopita, M. A., Leitherer, C., Davé, R., Yuan, T., Allen, M., Groves, B., & Sutherland, R. 2013, *ApJ*, 774, 100
- Kewley, L. J., & Ellison, S. L. 2008, *ApJ*, 681, 1183
- Kobulnicky, H. A., & Kewley, L. J. 2004, *ApJ*, 617, 240
- Kocevski, D., West, A. A., & Modjaz, M. 2009, *ApJ*, 702, 377
- Krühler, T., et al. 2015, *A&A*, 581, A125
- Küpcü Yoldaş, A., Salvato, M., Greiner, J., Pierini, D., Pian, E., & Rau, A. 2007, *A&A*, 463, 893
- Landolt, A. U. 1992, *AJ*, 104, 340
- Lara-López, M. A., et al. 2010, *A&A*, 521, L53
- Levan, A. J., Cenko, S. B., Perley, D. A., & Tanvir, N. R. 2013, *GRB Coordinates Network*, 14455
- Levan, A. J., et al. 2014a, *ApJ*, 781, 13
- . 2014b, *ApJ*, 792, 115
- Levesque, E. M., Berger, E., Kewley, L. J., & Bagley, M. M. 2010a, *AJ*, 139, 694
- Levesque, E. M., Berger, E., Soderberg, A. M., & Chornock, R. 2011, *ApJ*, 739, 23
- Levesque, E. M., Kewley, L. J., Berger, E., & Jabran Zahid, H. 2010b, *AJ*, 140, 1557
- Levesque, E. M., Kewley, L. J., Graham, J. F., & Fruchter, A. S. 2010c, *ApJL*, 712, L26
- Levesque, E. M., Soderberg, A. M., Kewley, L. J., & Berger, E. 2010d, *ApJ*, 725, 1337
- Maier, C., Ziegler, B. L., Lilly, S. J., Contini, T., Pérez-Montero, E., Lamareille, F., Bolzonella, M., & Le Floch, E. 2015, *A&A*, 577, A14
- Mangano, V., et al. 2007, *A&A*, 470, 105
- Mannucci, F., Cresci, G., Maiolino, R., Marconi, A., & Gnerucci, A. 2010, *MNRAS*, 408, 2115
- Mannucci, F., Salvaterra, R., & Campisi, M. A. 2011, *MNRAS*, 439
- Modjaz, M., et al. 2008, *AJ*, 135, 1136
- Morganti, R., et al. 2006, *MNRAS*, 371, 157
- Nakar, E. 2015, *ApJ*, 807, 172
- Niino, Y. 2011, *MNRAS*, 417, 567
- . 2012, *ApJ*, 761, 126
- Niino, Y., Choi, J., Kobayashi, M. A. R., Nagamine, K., Totani, T., & Zhang, B. 2011, *ApJ*, 726, 88
- Niino, Y., Nagamine, K., & Zhang, B. 2015, *MNRAS*, 449, 2706
- Ofek, E. O., Cenko, S. B., Gal-Yam, A., Peterson, B., Schmidt, B. P., Fox,

- D. B., & Price, P. A. 2006, GRB Coordinates Network, 5123
- Pagel, B. E. J., Edmunds, M. G., Fosbury, R. A. E., & Webster, B. L. 1978, *MNRAS*, 184, 569
- Perley, D. A., et al. 2013, *ApJ*, 778, 128
- . 2014, *ApJ*, 781, 37
- . 2016a, *ApJ*, 817, 7
- . 2016b, *ApJ*, 817, 8
- Price, P. A., Berger, E., & Fox, D. B. 2006, GRB Coordinates Network, 5275
- Prochaska, J. X., Bloom, J. S., Chen, H. W., Hurley, K., Dressler, A., & Osip, D. 2003, GRB Coordinates Network, 2482
- Prochaska, J. X., et al. 2004, *ApJ*, 611, 200
- Rosa, M. 1985, *The Messenger*, 39, 15
- Rossi, A., et al. 2014, *A&A*, 572, A47
- Sakamoto, T., et al. 2009, *ApJ*, 693, 922
- Salim, S., et al. 2007, *ApJS*, 173, 267
- Salvaterra, R., et al. 2012, *ApJ*, 749, 68
- Sánchez, S. F., et al. 2012, *A&A*, 538, A8
- Sanders, N. E., Caldwell, N., McDowell, J., & Harding, P. 2012, *ApJ*, 758, 133
- Savaglio, S., Glazebrook, K., & Le Borgne, D. 2009, *ApJ*, 691, 182
- Sawicki, M. 2012, *PASP*, 124, 1208
- Schlafly, E. F., & Finkbeiner, D. P. 2011, *ApJ*, 737, 103
- Schlesinger, K. J., et al. 2012, *ApJ*, 761, 160
- Schmidt, M. 2001, *ApJ*, 552, 36
- Schulze, S., et al. 2012, GRB Coordinates Network, 13257
- . 2014, *A&A*, 566, A102
- . 2015, *ApJ*, 808, 73
- Shields, G. A., & Searle, L. 1978, *ApJ*, 222, 821
- Sollerman, J., Östlin, G., Fynbo, J. P. U., Hjorth, J., Fruchter, A., & Pedersen, K. 2005, *New Astronomy*, 11, 103
- Stanek, K. Z., et al. 2006, *Acta Astronomica*, 56, 333
- Stanway, E. R., Levan, A. J., Tanvir, N., Wiersema, K., van der Horst, A., Mundell, C. G., & Guidorzi, C. 2015, *MNRAS*, 446, 3911
- Storey, P. J., & Zeppen, C. J. 2000, *MNRAS*, 312, 813
- Tanvir, N. R., Levan, A. J., Cucchiara, A., & Fox, D. B. 2012, GRB Coordinates Network, 13251
- Thöne, C. C., & de Ugarte Postigo, A. 2014, GRB Coordinates Network, 16079
- Thöne, C. C., et al. 2008, *ApJ*, 676, 1151
- Tinney, C., et al. 1998, *IAU Circ.*, 6896
- Tremonti, C. A., et al. 2004, *ApJ*, 613, 898
- Troja, E., Cusumano, G., Laparola, V., Mangano, V., & Mineo, T. 2006, *Nuovo Cimento B Serie*, 121, 1599
- Vergani, S. D., et al. 2015, *A&A*, 581, A102
- Wanderman, D., & Piran, T. 2010, *MNRAS*, 406, 1944
- Wolf, C., & Podsiadlowski, P. 2007, *MNRAS*, 375, 1049
- Woosley, S. E., & Heger, A. 2006, *ApJ*, 637, 914
- Xu, D., de Ugarte Postigo, A., Schulze, S., Jessen-Hansen, J., Leloudas, G., Kruehler, T., Fynbo, J. P. U., & Jakobsson, P. 2013a, GRB Coordinates Network, 14478
- Xu, D., et al. 2013b, *ApJ*, 776, 98
- Yates, R. M., Kauffmann, G., & Guo, Q. 2012, *MNRAS*, 422, 215
- Yoon, S., & Langer, N. 2005, *A&A*, 443, 643
- Zhang, B., Zhang, B.-B., Liang, E.-W., Gehrels, N., Burrows, D. N., & Mészáros, P. 2007, *ApJL*, 655, L25
- Zhang, B., et al. 2009, *ApJ*, 703, 1696
- Zhang, B.-B., et al. 2012, *ApJ*, 756, 190
- Zheng, W., Deng, J., & Wang, J. 2009, *Research in Astronomy and Astrophysics*, 9, 1103